# NACA

RESEARCH MEMORANDUM

LOW-SPEED AERODYNAMIC AND HYDRODYNAMIC CHARACTERISTICS OF

A PROPOSED SUPERSONIC MULTIJET WATER-BASED HYDRO-SKI

AIRCRAFT WITH UPWARD-ROTATING ENGINES

By William W. Petynia, Delwin R. Croom,
and Edwin E. Davenport

Langley Research Center
Langley Field, Va.

NATIONAL ADVISORY COMMITTEE
FOR AERONAUTICS
WASHINGTON

October 1958
Declassified August 19, 1960
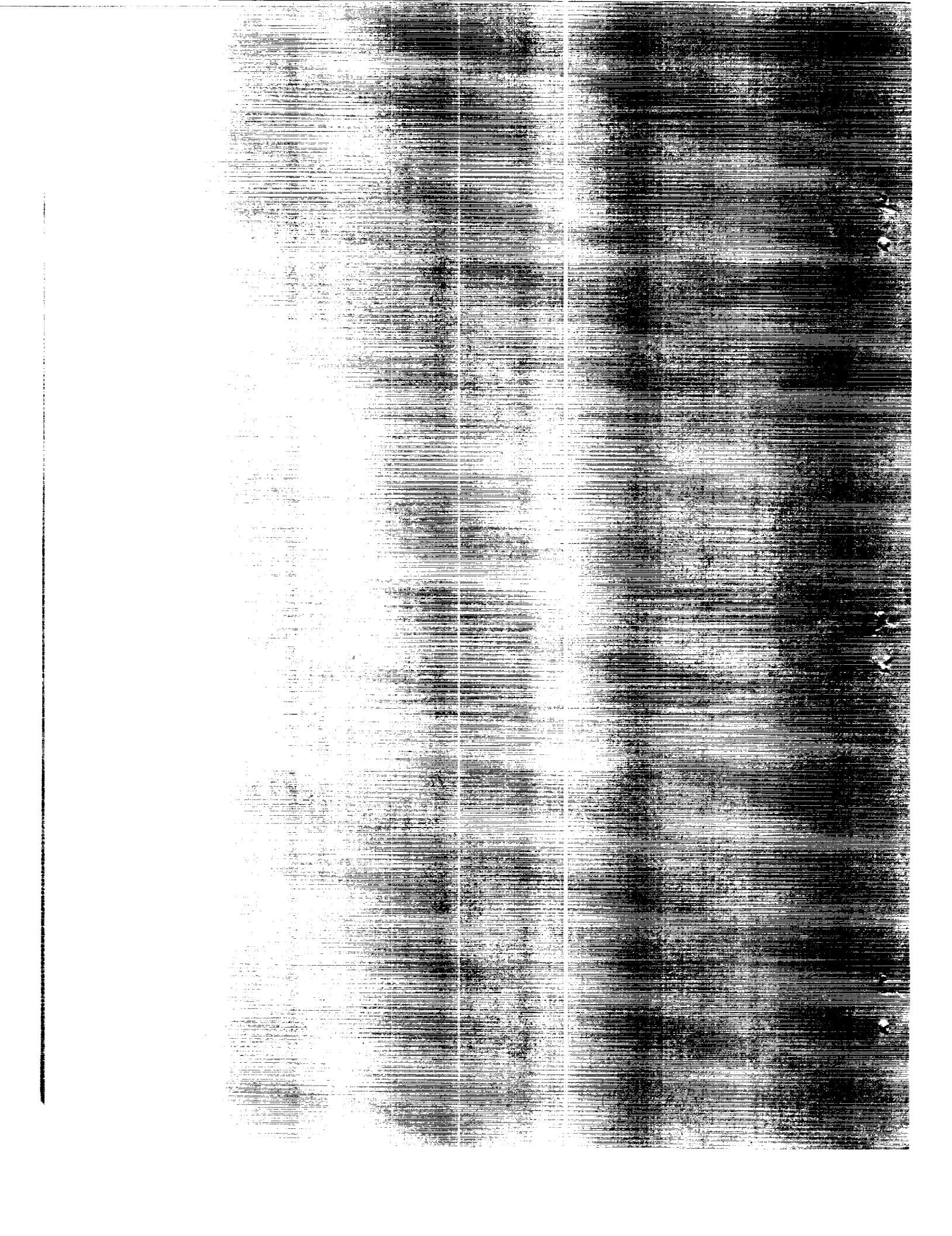
NATIONAL AERONAUTICS AND SPACE ADMINISTRATION

NASA MEMO 10-13-58L

LOW-SPEED AERODYNAMIC AND HYDRODYNAMIC CHARACTERISTICS OF A PROPOSED SUPERSONIC MULTIJET WATER-BASED HYDRO-SKI AIRCRAFT WITH UPWARD-ROTATING ENGINES*

By William W. Petynia, Delwin R. Croom,
and Edwin E. Davenport

SUMMARY

The low-speed aerodynamic and hydrodynamic characteristics of a proposed multijet water-based aircraft configuration for supersonic operation have been investigated. The design features include upward-rotating engines, body indentation, a single hydro-ski, and a wing with an aspect ratio of 3.0, a taper ratio of 0.143, 36.9° sweepback of the quarter-chord line, and NACA 65A004 airfoil sections.

For the aerodynamic investigation, with the flaps retracted, the model was longitudinally and directionally stable up to the stall. The all-movable horizontal tail was capable of trimming the model up to a lift coefficient of approximately 0.87. All flap configurations investigated had a tendency to become longitudinally unstable at stall. The effectiveness of the all-movable horizontal tail increased with increasing lift coefficient for all flap configurations investigated; however, with the large static margin of the configuration with the center of gravity at 0.25 mean aerodynamic chord, the all-movable horizontal tail was not powerful enough to trim all the various flapped configurations investigated throughout the angle-of-attack range.

For the hydrodynamic investigation, longitudinal stability during take-offs and landings was satisfactory. Decreasing the area of the hydro-ski 60 percent increased the maximum resistance and emergence speed 40 and 70 percent, respectively. Without the jet exhaust, the resistance was reduced by simulating the vertical-lift component of the forward engines rotated upward. However, the jet exhaust of the forward engines increased the maximum resistance approximately 60 percent. The engine inlets and horizontal tail were free from spray for all loads investigated and for both hydro-ski sizes.

---

*Title, Unclassified.

INTRODUCTION

The present investigation is part of a general research program undertaken at the Langley Aeronautical Laboratory to evaluate the aerodynamic and hydrodynamic capabilities of high-speed aircraft configurations suitable for supersonic flight and capable of operating from water bases. These configurations were characterized by low maximum cross-sectional area, high fineness ratio, and smooth area distribution to insure low subsonic and supersonic drag levels and a delayed drag rise. A description of the program and the design procedures used for one of these configurations is presented in reference 1. The results from wind-tunnel and tank investigations of the other configurations included in this research are presented in references 2 to 6.

The present configuration has a delta horizontal tail mounted high on the vertical tail and a midposition wing with an aspect ratio of 3.0, a taper ratio of 0.143, and 36.9° sweepback of the quarter-chord line. This wing-tail combination was found (ref. 7) to provide satisfactory aerodynamic stability characteristics over a wide range of lift coefficients. Two engines of the present model were mounted in pods under the leading edge of the wing. This engine location was selected on the basis of recent investigations which indicate an increase in flight lift-drag ratio at supersonic speeds (refs. 8 and 9) with the engines located so that they exhaust near the undersurface of the wing. The engines were rotated upward above the wing to provide necessary clearance while on the water.

The low-speed static aerodynamic longitudinal and lateral stability of the present configuration with several high-lift devices was determined in the Langley 300-MPH 7- by 10-foot tunnel. The hydrodynamic resistance, dynamic longitudinal stability during take-off and landing, and the spray characteristics were determined in the Langley tank no. 1. The effects of the hydro-ski size, engine rotational position, wing fuel tanks, and the jet exhaust of the forward engines upon the hydrodynamic characteristics were investigated.

COEFFICIENTS AND SYMBOLS

Aerodynamic

The static longitudinal aerodynamic data are referred to the wind axes and the static lateral aerodynamic data are referred to the body axes (fig. 1). All moments are referred to the wing 0.25 mean aerodynamic chord projected to the plane of symmetry.

C_D drag coefficient, $\dfrac{\text{Drag}}{qS}$

C_L lift coefficient, $\dfrac{\text{Lift}}{qS}$

C_Y side-force coefficient, $\dfrac{\text{Side force}}{qS}$

C_l rolling-moment coefficient, $\dfrac{\text{Rolling moment}}{qSb}$

C_n yawing-moment coefficient, $\dfrac{\text{Yawing moment}}{qSb}$

C_m pitching-moment coefficient, $\dfrac{\text{Pitching moment}}{qS\bar{c}}$

c wing chord, ft

$\bar{c}$ wing mean aerodynamic chord, $\dfrac{2}{S}\displaystyle\int_0^{b/2} c^2 dy$, ft

b wing span, ft

S wing area, sq ft

q free-stream dynamic pressure, $\rho V^2/2$, lb/sq ft

V free-stream velocity, ft/sec

ρ air density, slugs/cu ft

i_t angle of stabilizer incidence referred to hull baseline, positive when trailing edge down, deg

α angle of attack of hull baseline, deg

δ_f angle of flap deflection, positive deflection when trailing edge down, deg

δ_v angle of vane deflection, positive deflection when trailing edge down, deg

δ_n angle of leading-edge-flap deflection, measured in plane perpendicular to 0.20c line, deg

4

δ_N — wing-engine-nacelle angle of rotation referred to hull baseline, positive when engine is rotated upward, deg

β — angle of sideslip, deg

z — vertical distance, ft

x — longitudinal distance, ft

y — lateral distance, ft

$\dfrac{y_i}{b/2}$ — inboard end of flaps

$\dfrac{y_o}{b/2}$ — outboard end of flaps

$C_{l_\beta} = \left(\dfrac{\partial C_l}{\partial \beta}\right)_\alpha$ per degree

$C_{n_\beta} = \left(\dfrac{\partial C_n}{\partial \beta}\right)_\alpha$ per degree

$C_{Y_\beta} = \left(\dfrac{\partial C_Y}{\partial \beta}\right)_\alpha$ per degree

Abbreviations:

W — wing

F — fuselage

V — vertical tail

H — horizontal tail

Hydrodynamic

b — hydro-ski beam, ft

C_{Δ_0} — gross-load coefficient, Δ_0/wb^3

w   specific weight of water (63.3 lb/cu ft for these tests)

Δ_0 gross load, lb

τ angle of trim, angle between fuselage baseline and horizontal, deg

δ_e angle of elevator deflection, referred to stabilizer chord, positive when trailing edge down, deg

δ_s angle of stabilizer incidence, referred to fuselage baseline, positive when trailing edge down, deg

r   rise, vertical distance of center of gravity from free water surface set at zero with trailing edge of hydro-ski touching water surface when trim is zero; positive upward, ft

R   total resistance (including air drag), lb

Abbreviations:

c.g.   center-of-gravity location ($0.25\bar{c}$ for these tests)

L.W.L.   load water line

GENERAL CHARACTERISTICS OF CONFIGURATION

A general-arrangement drawing of the configuration and of the fuselage layout are presented in figures 2 and 3, respectively. Pertinent characteristics and dimensions of the proposed full-sized aircraft are presented in table I.

Basic Assumptions

The normal gross weight was assumed to be 180,000 pounds. A wing area of 2,000 square feet resulted in a wing loading of 90 lb/sq ft for the normal-gross-load condition. The addition of external wing tanks to provide additional fuel capacity and extended range increased the gross load to 200,000 pounds. Four turbojet engines, producing a total maximum sea-level thrust of 94,000 pounds, were selected. The bomb load was assumed to be 10,000 pounds.

Engine Location

The forward-engine nacelles were located in pods ahead of and below the wing. The two rearward engines were mounted in a single nacelle on the vertical tail and exhausted behind the tail surfaces. The two forward engine pods could be rotated upward to an angle of 45°. The axis of rotation passed through the center of gravity of the airplane to eliminate any change in thrust moment with engine rotation.

The location of the rearward engines afforded a favorable engine-inlet position from both aerodynamic and hydrodynamic considerations. The rearward location of the engines on the vertical tail also provided the weight distribution necessary for the longitudinal and vertical balance of the configuration.

Aerodynamic Considerations

The wing had an aspect ratio of 3.0, a taper ratio of 0.143, and 36.9° sweepback of the quarter-chord line. The wing had zero twist, an angle of incidence of 1.5°, and NACA 65A004 airfoil sections parallel to the free stream. The horizontal and vertical tails had NACA 65A006 airfoil sections.

Conventional double slotted, 30-percent-chord flaps extending from the 40-percent-semispan station to the tip were assumed for the basic configuration. Details of the flap (in cross section) are shown in figure 4.

The average cross-sectional-area curves for a Mach number of 1.4 for the complete configuration and for the various components are shown in figure 5. The method for obtaining the supersonic-area distribution was similar to that used in references 10 and 11. The longitudinal distribution of the components permits reduction in the cross-sectional area and also provides a smooth longitudinal distribution of this cross-sectional area with minimum fuselage indentation.

Hydrodynamic Considerations

No chines or chine strips were incorporated in the basic forebody to keep it as aerodynamically clean as possible. In order to provide a rearward hydrodynamic lifting element, a vee-bottom planing surface with an angle of dead rise of 10° and sharp chines was faired into the afterbody (fig. 3). The angles of the afterbody keel and chines to the forebody were kept small so that they would follow, as nearly as possible, the airstream flow lines and minimize the aerodynamic drag.

The single retractable hydro-ski was located with the trailing edge 2.0 feet forward of the center of gravity (0.25c̄) and 10.0 feet below the fuselage baseline (fig. 2). The center section of the hydro-ski conformed to the fuselage in cross section in the region of the retracted position and would retract flush with the fuselage bottom (fig. 6). The two outboard sections had an angle of dead rise of -10° which produced an effective angle of dead rise of approximately 0°. The hydro-ski size was determined for an emergence speed of 50 knots and an angle of trim of 2°. Data presented in reference 12, for a flat plate, were used to compute the required area of 227 square feet. The hydrodynamic lift of the wing and fuselage was neglected for computing the size of the basic hydro-ski (fig. 6).

Conventional tip floats were not necessary for this configuration, inasmuch as transverse stability at rest and at low speeds is provided by the wing. Tip skids might be required at intermediate water speeds if aileron control is inadequate.

MODELS

Wind Tunnel

A photograph of the model mounted on a single strut in the Langley 300-MPH 7- by 10-foot tunnel is presented in figure 7. The wing was equipped with either trailing-edge single slotted or double slotted flaps or both of various spans, leading-edge slats, and leading-edge flaps (see fig. 4 for details). The various double slotted flaps that were investigated had spans and deflections as follows:

$\dfrac{y_i}{b/2}$	$\dfrac{y_o}{b/2}$	δ_f, deg	Flap designation
0.074	0.397	40 to 60	Short span inboard
.074	.751	40 to 60	Medium span inboard
.397	1.000	42 to 53	Medium span outboard
.397	.751	42	Midspan

A single slotted flap having a deflection of 31° and extending from 0.074b/2 to 1.000b/2 and a combination of a single slotted and a double slotted flap were investigated (flap deflection of 26° for single slotted flap extending from 0.074b/2 to 0.397b/2; flap deflection of 53° for double slotted flap extending from 0.397b/2 to 0.751b/2.

For a few tests, wing fuel tanks were mounted on pylons underneath the wings and the wing-engine nacelles were pivoted about the point shown in figure 2. The model had an all-movable horizontal tail which pivoted about the 50-percent-chord point of the tail root chord.

Tank Model

Photographs of the 1/15-size dynamic model used for the hydrodynamic investigation in the Langley tank no. 1 are presented in figure 8.

The fuselage was constructed of plastic-impregnated fiber glass and the tail surfaces were of conventional wood and silk construction. The hydro-ski, wing, and flaps were made of wood and were covered with a heat-resistant plastic-impregnated fiber glass cloth. The lenticular hydro-ski struts were made of aluminum.

Aluminum leading-edge slats were used to prevent premature wing stall that is usually encountered at the low Reynolds numbers of the tank tests. Medium-span outboard flaps were used for the tank model. The flaps could be fixed at deflections of 0°, 30°, 40°, and 50°. Details of the leading-edge slats and trailing-edge flaps are shown in figure 4. The horizontal tail and elevators could be fixed at angles of 5° to -15° and 20° to -20°, respectively.

The forward-engine pods could be rotated upward to angles of 45° during the test by means of an electric motor located within the model. Thrust for the two forward engines was provided by hydrogen peroxide decomposition-type motors. The motors and apparatus necessary for the operation of the motors were the same as those used in reference 6. The two rearward engines were unpowered.

Electric contacts were located on the model at the sternpost and the trailing edge of the hydro-ski to indicate when these portions of the model were in the water. These electric contacts also were used to release the trim brake during the landing tests.

APPARATUS AND TESTS

Aerodynamic

The tests to determine the static longitudinal and lateral aerodynamic characteristics of the model with the hydro-ski removed were made on the single-strut support system in the Langley 300-MPH 7- by 10-foot tunnel. Longitudinal aerodynamic tests, and the lateral aerodynamic tests at $\beta = \pm 4^\circ$, with the flaps retracted were made at a

dynamic pressure of approximately 45 lb/sq ft, corresponding to an air-speed of about 194 ft/sec. The lateral tests with the flaps extended, the lateral test through the sideslip-angle range with flaps retracted, and the longitudinal tests with the flaps extended were made at a dynamic pressure of approximately 28 lb/sq ft, corresponding to an airspeed of about 153 ft/sec. Reynolds numbers for these airspeeds of 194 and 153 ft/sec, based on the wing mean aerodynamic chord, were approximately 2.37×10^6 and 1.84×10^6, respectively. The angle-of-attack range for the flaps-retracted configuration was from about -4° through the stall, and for the flaps-extended configuration it was from about -8° through the stall.

Hydrodynamic

The hydrodynamic investigation was made in Langley tank no. 1, which is described in reference 13. The apparatus and procedure used to investigate the hydrodynamic characteristics of the model are similar to those described in reference 14. A photograph of the setup of the model on the towing apparatus is presented in figure 9.

The model was free to trim about the center of gravity and to move vertically, but it was restrained laterally and in yaw and roll for all the tests. Slide-wire pickups were used to record the trim and rise. Trim was referenced to the fuselage baseline and the undisturbed water surface. Rise of the center of gravity was set at zero with the hydro-ski touching the water with the fuselage at zero trim.

The resistance of the complete model, including air drag, was determined with and without power (with and without the effects of the jet exhaust simulated) at constant speeds up to the take-off for a range of tail settings and two flap positions. Without power, the thrust moment was simulated by a static moment and the vertical-thrust component due to the forward-engine rotational position was simulated by a reduction in the gross weight. In addition, for some power-off tests the effect of the model trim on the vertical-thrust component was considered in order to compare it with the effect in power-on tests. During tests with power, scale thrust for the forward engines was provided by the hydrogen peroxide rocket motors. The thrust moment and lift component of the unpowered rearward engines were simulated as befor Photographs and observations were made of the spray patterns during these tests.

Take-off stability was determined during constant-speed and accelerated tests with and without power at a weight corresponding to the design gross load of 180,000 pounds. Without power, the forces and moments were simulated in the same manner as those of the power-off

resistance tests. The load on the water was corrected for an average trim during the acceleration to take-off speed. A maximum constant acceleration of $4\frac{1}{2}$ ft/sec^2 was used for the take-offs. During the take-off the engines were held in the 30° up position with the flaps retracted until a speed of 70 knots was obtained (full-size). Above this speed the engines were lowered to the flight position and the flaps were extended.

Landings were made with the flaps extended and the engines down. All landings were assumed to be power off and no forces or moments were simulated. The model was fixed in trim at the desired landing trim at speeds greater than the flying speed of the model. The carriage was decelerated at a uniform rate and the model glided onto the water. Upon contact with the water surface the trim brake was released to permit freedom in trim. The engines were rotated upward and the flaps retracted during the landing runout. Slide-wire pickups were used to obtain records of the trim and rise, and motion pictures were taken during the landings.

CORRECTIONS

Aerodynamic

The aerodynamic values of angles of attack, drag coefficients, and pitching-moment coefficients which were obtained in the Langley 300-MPH 7- by 10-foot tunnel have been corrected for jet-boundary effects by the method of reference 15.

The data have been corrected for tunnel air-flow misalinement, tunnel blockage, and longitudinal pressure gradient in the tunnel. Tare corrections for the single-support strut have not been applied to these data.

Hydrodynamic

The hydrodynamic resistance data presented are the net resistance with the drag of the towing staff and power leads subtracted as a tare.

RESULTS AND DISCUSSION OF AERODYNAMIC DATA

The basic aerodynamic data for the model are presented in figures 10 to 15 for the flaps-retracted condition and in figures 16 to 24 for the flaps-extended condition.

Static Longitudinal Stability Characteristics

Trailing-edge flaps retracted.- The static longitudinal stability characteristics in pitch of the model with trailing-edge flaps retracted at several stabilizer incidences are given in figure 10. No abrupt break in lift curve was noted for the model, the model was longitudinally stable, and the all-movable horizontal tail was capable of trimming the model up to a lift coefficient of about 0.87.

The effect of leading-edge-flap deflection and wing-engine nacelles on the pitch characteristics of the model are presented in figure 11. The addition of the wing-engine nacelles at 0° caused a slight decrease in longitudinal stability; when the leading-edge flaps and wing-engine nacelles were deflected $\left(\delta_n = 5^\circ \text{ and } \delta_N = 15^\circ\right)$, longitudinal instability was noted at the stall. The basic wing and fuselage became longitudinally unstable at the stall; however, deflecting the leading-edge flaps with the addition of wing-engine nacelles resulted in longitudinal stability throughout the angle-of-attack range.

Trailing-edge flaps extended.- Increasing the span of the inboard double slotted flap from short span (fig. 16) to medium span (fig. 17) resulted in an increase in the maximum untrimmed lift coefficient from 1.30 to 1.43. The maximum lift coefficient occurred at a lower angle of attack $\left(\alpha \approx 13^\circ \text{ as compared with } \alpha \approx 7^\circ\right)$, and much higher values of lift coefficient in the negative and small angle-of-attack range were obtained $\left(C_L \text{ of } 0.72 \text{ at } \alpha = 0^\circ \text{ as compared with } 1.17\right)$. Larger nose-down pitching moments and a reduction in longitudinal stability (reduction in static margin of about 5 percent) resulted from the increase in flap span; however, longitudinal instability was noted for both spans of the flap at the stall.

When the medium-span outboard double slotted flap was used on the model, the lift curves became nonlinear and longitudinal instability was noted at a lift coefficient of about 0.9 with slats off (fig. 18). These nonlinearities probably were caused by an earlier stall of the outboard portion of the wing resulting from the added load from the double slotted flap. As the wing tip stalled, the center of load moved forward and the model became longitudinally unstable. The linear-lift-curve range was extended and the longitudinal stability was relatively unaffected when leading-edge slats were installed on the model; however, longitudinal instability was still evident at a lift coefficient of about 1.17. A midspan double slotted flap was tested at a flap deflection of 42° with the slats installed (fig. 19). The lift curve for this configuration was linear up to a lift coefficient of about 1.2, and the model showed a longitudinal instability tendency at a lift coefficient of about 1.2.

When full-span single slotted flaps and a leading-edge slat were used (fig. 20), the lift curve was more linear up to the stall than the lift curve of the aforementioned medium-span outboard double-slotted-flap arrangement (fig. 18), and a lift coefficient of about 1.34 was reached before longitudinal instability was evident; however, the static margin was reduced about 7 percent.

A combination of a double slotted flap, a single slotted flap, and a leading-edge slat was investigated that gave a fairly linear lift curve (fig. 22). The maximum untrimmed lift coefficient for this configuration was on the order of 1.5, and the model became longitudinally unstable as the model stalled.

Some evidence of the all-movable horizontal-tail effectiveness $-dC_m/di_t$ is shown in figures 19 to 22 for the model equipped with mid-span double slotted flaps, full-span single slotted flaps, medium-span outboard double slotted flaps, and a combination of double slotted and single slotted flaps. The effectiveness of the all-movable horizontal tail $-dC_m/di_t$ increased with increased lift coefficient. For the configuration consisting of a combination of a double slotted and single slotted flap, however, it is evident that at low angles of attack the horizontal tail has stalled; in order to trim this configuration about the center of gravity $(0.25\bar{c})$ at low angles of attack, modifications to the horizontal tail would be in order - either enlarge the tail, relocate the tail, or equip the tail with high-lift devices. It should be noted, however, that the static margin for these tests was on the order of 13 to 21 percent, and if a lower static margin was assumed (move center of gravity rearward), the horizontal tail could possibly trim all the configurations tested.

A comparison of the estimated trim lift coefficients for the basic model and for the model with various flap configurations is made in figure 25. These data indicate that the combination of double slotted and single slotted flaps would give the largest value of maximum trim lift coefficient $\left(C_{L,trim} = 1.35\right)$.

Static Lateral Stability Characteristics

Trailing-edge flaps retracted.- The static lateral stability characteristics of the trailing-edge flap-retracted model at several angles of attack are presented in figure 12. The variation of C_n, C_Y, and C_l with β was linear from about $\beta = \pm 5°$. The directional stability decreased with increased angle of attack, and a small decrease in directional stability resulted from deflection of the leading-edge flap and

the wing-engine nacelles. The model became directionally unstable beyond a sideslip angle of about 15°. The side-force coefficient C_Y increased in magnitude with increase in sideslip angle.

The rolling-moment coefficient increased negatively with increase in sideslip angle over the angle-of-attack range from 0.2° to 8.6°, and a slight decrease in rolling moment was noted because of deflection of leading-edge flaps and wing-engine nacelles. As the angle of attack was increased to 16.9°, the magnitude of rolling moment was decreased.

The data of figures 13, 14, and 15 are in the form of slopes obtained from values of C_n, C_Y, and C_l at $\beta = \pm 4^\circ$ as the model is tested through the angle-of-attack range. The variation of side-force coefficient with sideslip angle C_{Y_β} remained about constant through the angle-of-attack range for all configurations tested, except for the configuration with wing-engine nacelles removed which showed a decrease in C_{Y_β} beyond the stall.

The directional stability C_{n_β} decreased as the angle of attack was increased for all flaps-retracted configurations tested (fig. 13). Either addition of the external mounted wing fuel tanks or the deflection of the leading-edge flaps generally caused a slight increase in the directional stability of the model. At angles of attack below the stall, the addition of wing-engine nacelles caused a decrease in directional stability. The basic model (trailing-edge flap retracted) with or without the horizontal tail was directionally stable up to the stall (fig. 15); however, the horizontal tail added appreciably to the directional stability of the model because of the end-plate effects of the tee-tail. The basic fuselage and the wing-fuselage combination with or without the wing-engine nacelles were directionally unstable.

The effective dihedral C_{l_β} for all flaps-retracted configurations tested increased negatively as the angle of attack was increased from about -5° to about 7°; above $\alpha \approx 7^\circ$ up to the stall, a decrease in magnitude of C_{l_β} was noted. The rather large values of effective dihedral $-C_{l_\beta}$ in the low and moderate angle-of-attack range as indicated in figures 13, 14, and 15 for the complete model were caused by the empennage. (See fig. 15.)

Trailing-edge flaps extended.- The static lateral aerodynamic characteristics of the combination of a double slotted and single slotted flap at several angles of attack are presented in figure 23. The data of figure 24 are in the form of slopes obtained from values of C_n, C_Y,

and C_l at $\beta = \pm 4°$ as the model is tested through the angle-of-attack range. The variation of side-force coefficient with sideslip angle C_{Y_β} increased negatively as the angle of attack was increased. The directional stability C_{n_β} increased as the angle of attack was increased from $-7\frac{1}{2}°$ to $0°$ and remained constant from $\alpha = 0°$ to beyond the stall. The effective dihedral C_{l_β} increased negatively with angle of attack up to about $7°$ and then decreased as the wing stalled.

RESULTS AND DISCUSSION OF HYDRODYNAMIC DATA

Resistance

Power off.- The power-off total resistance, trim, and rise for a normal gross load of 180,000 pounds is shown in figure 26 with the flaps, stabilizer, and elevator set at zero deflection. Also presented are several other load conditions for speeds up through the emergence speed of the hydro-ski. These loads correspond to the gross load corrected for the vertical-lift component of the forward engines when rotated upward $22\frac{1}{2}°$, $30°$, and $45°$. The total resistance and emergence speed were reduced by rotating the engines $22\frac{1}{2}°$. Further rotation, to angles up to $45°$, reduced the resistance only slightly below that obtained at $22\frac{1}{2}°$ and had practically no effect on the trim, rise, or emergence speed. After emergence, with the normal gross load (no lift component due to engine rotation), the resistance increased with speed up to 70 knots. This increase was caused by heavy spray from the chines of the hydro-ski striking the under side of the wing and fuselage. For speeds greater than 70 knots, the resistance and trim decreased with speed. A small oscillation in trim was noted between 75 and 100 knots.

The total resistance, trim, and rise with external wing tanks and a gross load of 200,000 pounds are presented in figure 27. This configuration is compared with the configuration without wing tanks at 180,000 pounds. The wing tanks, with the associated increase in gross load, increased the resistance and trim prior to the emergence but decreased the emergence speed. After emergence, the wing tanks were clear of the water and the only penalty to the hydrodynamic characteristics would be that associated with the increase in gross load.

The emergence speeds shown in figures 26 and 27 were lower than those calculated on the basis of hydro-ski lift as a result of the hydrodynamic lift of the wing and fuselage. The effect of a 60-percent

reduction in the area of the hydro-ski, therefore, was investigated by removing 22.5 feet of the length from the constant center section of the hydro-ski. By reducing the hydro-ski area in this manner, the same beam and beam loading were maintained for the two hydro-skis. After emergence the short hydro-ski would, therefore, exhibit the same resistance and stability as the original large hydro-ski, since the longitudinal position of the trailing edge was held constant.

The total resistance and trim for the large hydro-ski and for the short hydro-ski with chine strips (fig. 3) on forebody are shown in figure 28 with the lift component of the thrust simulated as before. Without the forebody chine strips, a considerable increase in the emergence speed and an increase in spray and forebody wetting were noted with the short hydro-ski. In order to alleviate this wetting and consequent increased resistance, spray strips were added to the forebody. The addition of the spray strips increased the trim and decreased the resistance with the short hydro-ski. It is seen that the maximum resistance and emergence speed of the short hydro-ski are greater by approximately 40 and 70 percent, respectively, than those of the large hydro-ski.

Power on.- The effect of the jet exhaust of the forward engines on the total resistance and trim of the configuration with the short hydro-ski is presented in figure 29. For comparison, power-off data with the vertical component of the thrust due to engine rotation and the thrust moment simulated also are presented. Flaps deflected 0° and 50° and two stabilizer-elevator deflections are shown for both the power-off and power-on conditions.

At speeds prior to emergence, the principal effect of the jet was to accelerate the spray under the wing and increase the maximum resistance approximately 60 percent. The trims just prior to emergence were decreased about $\frac{1}{2}^o$ and the emergence speed was increased approximately 5 knots. Attempts to direct the jet in a more horizontal direction by canting the tailpipe had little effect on the trim or resistance.

After emergence, the power-on resistance (with the flaps retracted and 0° tail setting) was only slightly greater than with power off. The effect of the forward jets would be expected to be small at these speeds since wing wetting was reduced after emergence by the clearance provided by the hydro-ski. A small-amplitude oscillation in trim was noted at some speed intervals between emergence and 120 knots as indicated by crosshatching.

With the flaps deflected 50°, greater stabilizer-elevator settings were used (-10°, -20°, respectively) to overcome the usual bow-down

moment produced by flap deflection. Deflection of the flaps increased
the total resistance for both the power-off and power-on conditions.
The increase in the total resistance with flap deflection was due primar-
ily to the aerodynamic drag of the flap since adequate spray clearances
for the 60-percent-span, 30-percent-chord flaps were provided by the
hydro-ski. After emergence, the increase in resistance due to power
was slightly greater with flaps deflected than with the flaps retracted.
A small decrease in trim due to power is shown throughout the speed
range. Since the total resistance increased with flap deflection, it
would be desirable to deflect the flaps as late in the take-off as prac-
ticable. The full-span, small-chord flap (fig. 25) would provide greater
lift for take-off and landing than the partial-span flap, and the addi-
tional inboard portion of the flap would be relatively clear of spray
at high speeds.

Stability

Trim limits.- The power-off trim limits of stability are presented
in figure 30 with no thrust moments or forces simulated. The lower trim
limit of stability which is shown for the basic hydro-ski would be the
same for the short hydro-ski in the region of speeds shown. The calcu-
lated minimum trim at which the hydro-ski lift would support the load
on the water is shown for both hydro-skis. As the aircraft is trimmed
down from the stable planing region, the lower limit of stability would
be encountered before the minimum planing trim; but should the amplitude
of porpoising be allowed to increase until the minimum planing trim was
reached, the hydro-ski would submerge. The maximum attainable trims
for a center-of-gravity location of $0.25\bar{c}$ and the maximum stabilizer-
elevator deflection are shown. No upper stability limit was found below
these trims.

Smooth-water take-offs.- Variations in trim during acceler-
ated smooth-water take-offs are presented in figure 31 for several
stabilizer-elevator deflections with flaps deflected 0° and 50° with
power on and power off. The vertical component of the thrust due to
engine rotation was simulated for power-off conditions. The variations
in trim for two rates of longitudinal acceleration through emergence
are shown to illustrate the effect of acceleration on the tendency for
the model to oscillate in trim at emergence. With the lower rate of
forward acceleration, the model emerges onto the hydro-ski more gradually
with less vertical motion than with the higher rates of acceleration;
thus, a smaller trim oscillation is induced as the hydro-ski seeks a
trim equilibrium after emergence. Once on the hydro-ski, the trim remained
high until a speed of approximately 95 knots was attained at which speed
aerodynamic control became effective. A wide range of trims was avail-
able for take-off.

With the model planing on the hydro-ski, a small-amplitude trim oscillation of relatively high frequency (1 cycle/sec) may be noted at trims near the sternpost angle where the afterbody contacts the water surface during the oscillation. The jet exhaust appeared to increase slightly the amplitude of this oscillation at high speeds. This oscillation was not divergent and did not appear at angles of trim lower than the sternpost angle with the afterbody clear of the water surface.

At speeds greater than 95 knots, with 0° flap deflection, the model could be trimmed below the sternpost angle. In this same speed region, deflection of the flaps to 50° imposed a nose-down pitching moment which resulted in trims below the sternpost angle for all stabilizer-elevator deflections. A long-period oscillation of small amplitude was noted in this region of trims and speeds.

Smooth-water landings.- Smooth-water landings were made over a range of landing trims from 7° to 15° at a normal take-off gross load of 180,000 pounds. The variations in trim and rise for two typical smooth-water landings at trims greater and less than the sternpost angle are presented in figure 32. At landing trims less than the sternpost angle (fig. 32(a)), very little change in trim or rise was noted. As the model trimmed about the sternpost at the initial impact at landing trims greater than the sternpost angle (fig. 32(b)), a pitching oscillation was induced which damped out during the runout and the landing appeared stable. The pitch oscillation damped in a manner similar to the pitching oscillation encountered during take-offs at trims near the sternpost angle.

Spray Characteristics

Photographs of the spray for the configuration with the short hydro-ski are presented in figures 33 and 34 for conditions without and with power, respectively. The engines were rotated 30°, since at preemergence speeds the afterportions of the nacelles were heavily wetted by spray at smaller angles of rotation.

Power off.- With the power off (fig. 33), the trailing edge and outboard portions of the wing were under water in the static condition. At low speeds, the wing was heavily wetted; a spray blister which emanated from the leading edge of the wing was thrown over the top and outboard portion of the wing. At speeds greater than 50 knots, the model was planing on the under surface of the wing with the leading edge clear of the water surface (fig. 33(d)). At speeds up to the emergence speed, the forebody sides were heavily wetted by flow clinging to the sides and flowing back over the fuselage and wing. However, the addition of chine strips reduced this wetting. The sharp increase in trim and

rise at emergence (characteristic of hydro-skis) caused the flow to break clear from the forebody and afterbody sides above the chines.

A similar spray pattern was observed with the large hydro-ski. The greater hydro-ski area increased the trim at the lower speeds before emergence and both the amount and duration of the spray were reduced. The flow clinging to the smooth forebody sides did not appear to be excessive and spray strips were not used.

For both hydro-ski configurations, the under surface of the wing was heavily wetted by the spray from the hydro-ski just after emergence. Flaps extended in this speed range would be subject to the heavy spray blister from the hydro-ski. At speeds greater than 85 knots, the wing was free of the heavy spray blister, and the flaps were practically free of spray at a speed of 92 knots (fig. 33(e)).

Power on.- Photographs of the spray with the power on are presented in figure 34. At speeds below emergence, power had no significant effect upon the flow on the forebody sides. Spray was thrown against the under side of the wing by the jet exhaust striking the water surface. After emergence there was no apparent effect of power on the spray (fig. 34(f)).

The horizontal tail and the engine inlets were free from spray throughout the speed range for both hydro-ski configurations. The addition of wing fuel tanks for the overload condition of 200,000 pounds produced no significant changes in the spray.

CONCLUDING REMARKS

Aerodynamic

In the aerodynamic investigation the longitudinal and directional stability characteristics were generally satisfactory for the basic model (flaps retracted). The all-movable horizontal tail was capable of trimming the basic model up to a lift coefficient of approximately 0.87.

All flap configurations investigated had a tendency to become longitudinally unstable at the stall. A combination of an inboard single slotted flap, an outboard double slotted flap, and a leading-edge slat gave the highest maximum lift coefficient, and the model in this configuration was directionally stable throughout the angle-of-attack range.

The effectiveness of the all-movable horizontal tail increased with increasing lift coefficient for all flap configurations investigated; however, with the large static margin of the configuration with the center

of gravity at 0.25 mean aerodynamic chord, the basic all-movable horizontal tail was not powerful enough to trim all the various flapped configurations investigated throughout the angle-of-attack range.

Hydrodynamic

In the hydrodynamic investigation the maximum take-off resistance occurred just before emergence onto the hydro-ski. Decreasing the area of the hydro-ski 60 percent increased the maximum resistance and the emergence speed 40 and 70 percent, respectively. Without the jet exhaust, the total resistance and emergence speed were reduced by simulating the vertical-lift component of the forward engines rotated upward. However, the jet exhaust of the forward engines increased the maximum resistance approximately 60 percent by accelerating the spray which impinged on the under side of the wing and fuselage. The addition of external wing fuel tanks to increase the gross load increased resistance before emergence but reduced emergence speed.

A wide range of stable trims was available for take-offs and landings. The engine inlets and horizontal tail were free from spray for all loads investigated and for both hydro-ski sizes.

Langley Research Center,
    National Aeronautics and Space Administration,
        Langley Field, Va., July 23, 1958.

REFERENCES

1. Petynia, William W., Hasson, Dennis F., and Spooner, Stanley H.:
   Aerodynamic and Hydrodynamic Characteristics of a Proposed Super-
   sonic Multijet Water-Based Hydro-Ski Aircraft With a Variable-
   Incidence Wing. NACA RM L57G05, 1957.

2. Olson, Roland E., and Bielat, Ralph P.: An Aerodynamic and Hydro-
   dynamic Investigation of Two Multijet Water-Based Aircraft Having
   Low Transonic Drag Rise. NACA RM L55A11a, 1955.

3. McKann, Robert E., and Coffee, Claude W.: Limited Hydrodynamic
   Investigation of a 1/15-Size Model of a Modified Nose-Inlet Multi-
   jet Water-Based Aircraft. NACA RM L55J19, 1956.

4. Bielat, Ralph P., Coffee, Claude W., Jr., and Petynia, William W.:
   Aerodynamic and Hydrodynamic Characteristics of a Deck-Inlet Multi-
   jet Water-Based-Aircraft Configuration Designed for Supersonic
   Flight. NACA RM L56H01, 1956.

5. Morse, Archibald E., Jr., Woodward, David R., and Blanchard,
   Ulysse J.: An Investigation of the Hydrodynamic Characteristics
   of a Dynamic Model of a Transonic Seaplane Design Having a Planing-
   Tail Hull. NACA RM L56C28a, 1956.

6. Blanchard, Ulysse J.: Hydrodynamic Investigation of a Model of a
   Supersonic Multijet Water-Based Aircraft With Engines Exhausting
   From the Step. NACA RM L57F20, 1957.

7. Few, Albert G., Jr.: Investigation at High Subsonic Speeds of the
   Static Longitudinal Stability Characteristics of a Model Having
   Cropped-Delta and Unswept Wing Plan Forms and Several Tail Con-
   figurations. NACA RM L55I23a, 1955.

8. Falanga, Ralph A., and Judd, Joseph H.: Flight Investigation of the
   Effect of Underwing Propulsive Jets on the Lift, Drag, and Longitu-
   dinal Stability of a Delta-Wing Configuration at Mach Numbers From
   1.23 to 1.62. NACA RM L55I13, 1955.

9. Bressette, Walter E., and Faget, Maxime A.: An Investigation of Jet
   Effects on Adjacent Surfaces. NACA RM L55E06, 1955.

10. Hoffman, Sherwood, Wolff, Austin L., and Faget, Maxime A.: Flight
    Investigation of the Supersonic Area Rule for a Straight Wing-Body
    Configuration at Mach Numbers Between 0.8 and 1.5. NACA RM L55C09,
    1955.

11. Whitcomb, Richard T.: Some Considerations Regarding the Application of the Supersonic Area Rule to the Design of Airplane Fuselages. NACA RM L56E23a, 1956.

12. Weinstein, Irving, and Kapryan, Walter J.: The High-Speed Planing Characteristics of a Rectangular Flat Plate Over a Wide Range of Trim and Wetted Length. NACA TN 2981, 1953.

13. Truscott, Starr: The Enlarged N.A.C.A. Tank, and Some of Its Work. NACA TM 918, 1939.

14. Olson, Roland E., and Land, Norman S.: Methods Used in the NACA Tank for the Investigation of the Longitudinal-Stability Characteristics of Models of Flying Boats. NACA Rep. 753, 1943. (Supersedes NACA WR L-409.)

5. Gillis, Clarence L., Polhamus, Edward C., and Gray, Joseph L., Jr.: Charts for Determining Jet-Boundary Corrections for Complete Models in 7- by 10-Foot Closed Rectangular Wind Tunnels. NACA WR L-123, 1945. (Formerly NACA ARR L5G31.)

TABLE I

PERTINENT CHARACTERISTICS AND DIMENSIONS OF

THE FULL SIZE WATER BASED AIRCRAFT

General:
Gross weight, lb 180,000
Wing area, sq ft 2,000
Engines 4
Take-off thrust (with afterburners), lb 94,000
Take-off wing loading, lb/sq ft 90
Take-off thrust-weight ratio 0.52
Total surface area, sq ft 9,595

Wing:
Span, ft 77.53
Wing area, sq ft 2,000
Airfoil section . . . . NACA 65A004
Aspect ratio 3.0
Taper ratio 0.143
Sweepback (0.25$\bar{c}$), deg 36.9
Dihedral, deg 0
Length, mean aerodynamic chord, ft 30.67
Incidence, deg 1.5
Twist, deg 0

Horizontal tail:
Span, ft 35.0
Airfoil section . . . . NACA 65A006
Area, sq ft 306.3
Aspect ratio 4.0
Taper ratio 0
Sweepback (0.25$\bar{c}$), deg 36.9
Dihedral, deg 0
Arm, between 0.25$\bar{c}$ of wing to 0.25$\bar{c}$ of horizontal tail, ft 47.68

Vertical tail:
Airfoil section . . . . NACA 65A006
Aspect ratio 1.18
Sweepback (0.25$\bar{c}$), deg 38.8

Fuselage:
Length, overall, ft 145.2
Width, maximum, ft 6.6
Height, maximum, ft 11.85
Afterbody dead rise, deg 10.0
Sternpost angle, deg 2.0
Center of gravity above fuselage baseline, ft 8.15

Area curve:
Maximum net cross-sectional area, sq ft 100
Maximum diameter of equivalent body, ft 11.28
Length, ft 145.2
Fineness ratio of equivalent body 12.9

	Basic	Reduced length
Hydro-ski:		
Maximum length, ft	44.0	21.5
Maximum beam, ft	6.0	6.0
Length-beam ratio	7.33	3.58
Area, sq ft	227.4	92.4
Beam-loading coefficient, C_{Δ_0}	13.1	13.1
$\dfrac{\text{Gross weight}}{\text{Hydro-ski area}}$, lb/sq ft	791.5	1,948.0
Incidence, deg	2	2
Distance of trailing edge below fuselage baseline, ft	10.0	10.0
Distance of trailing edge ahead of 0.25$\bar{c}$, ft	2.03	2.03
Sternpost angle, deg	10.75	10.75
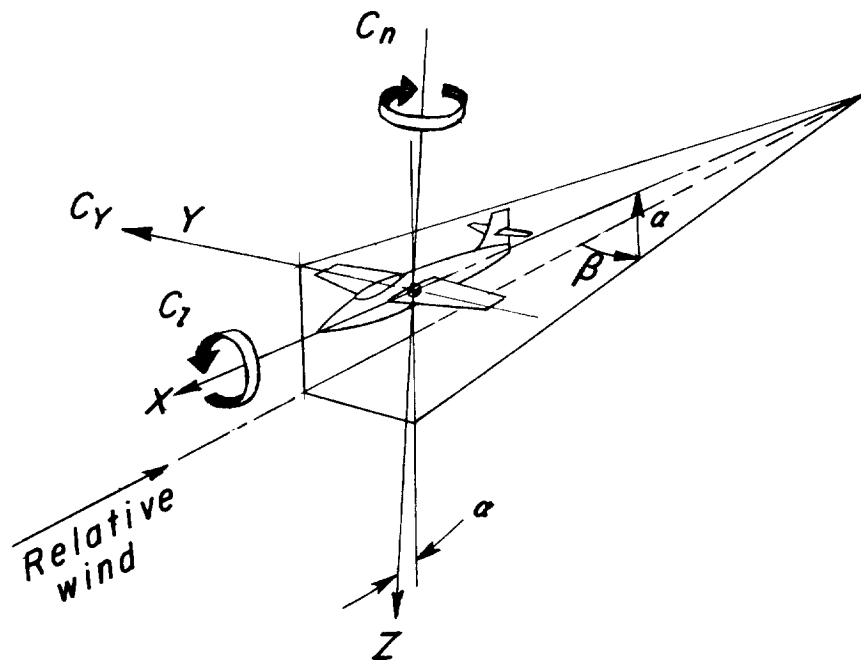
(a) Body axis.
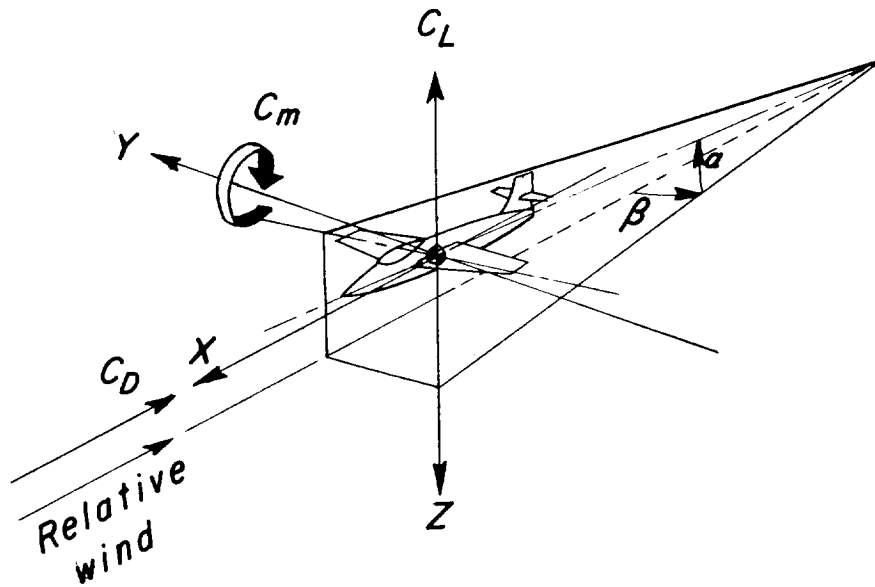
(b) Wind axis.

Figure 1.- Systems of axes showing direction and sense of forces, moments, and angular quantities.

24
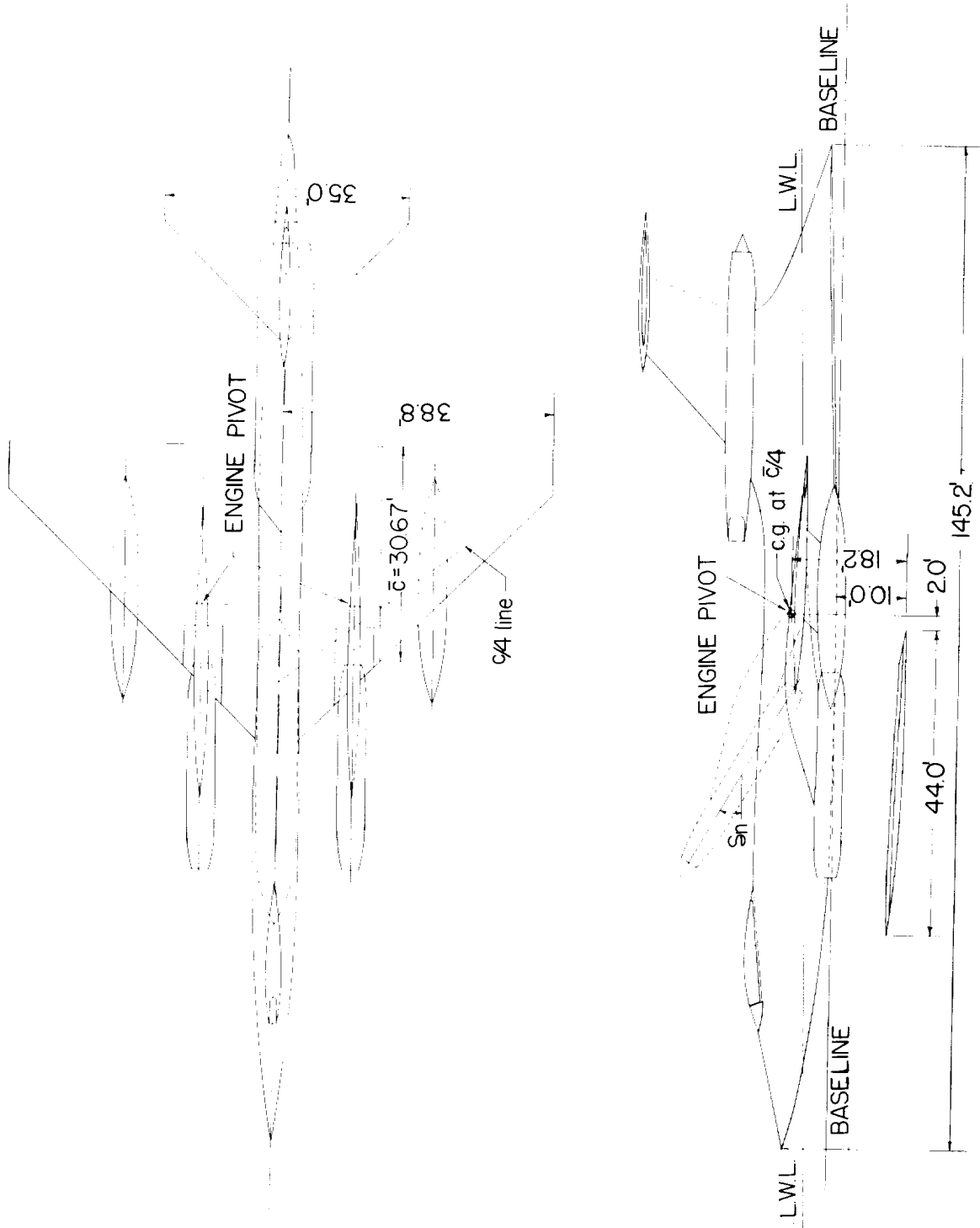
Figure 2.- General arrangement of configuration.

Z

CHINE STRIP
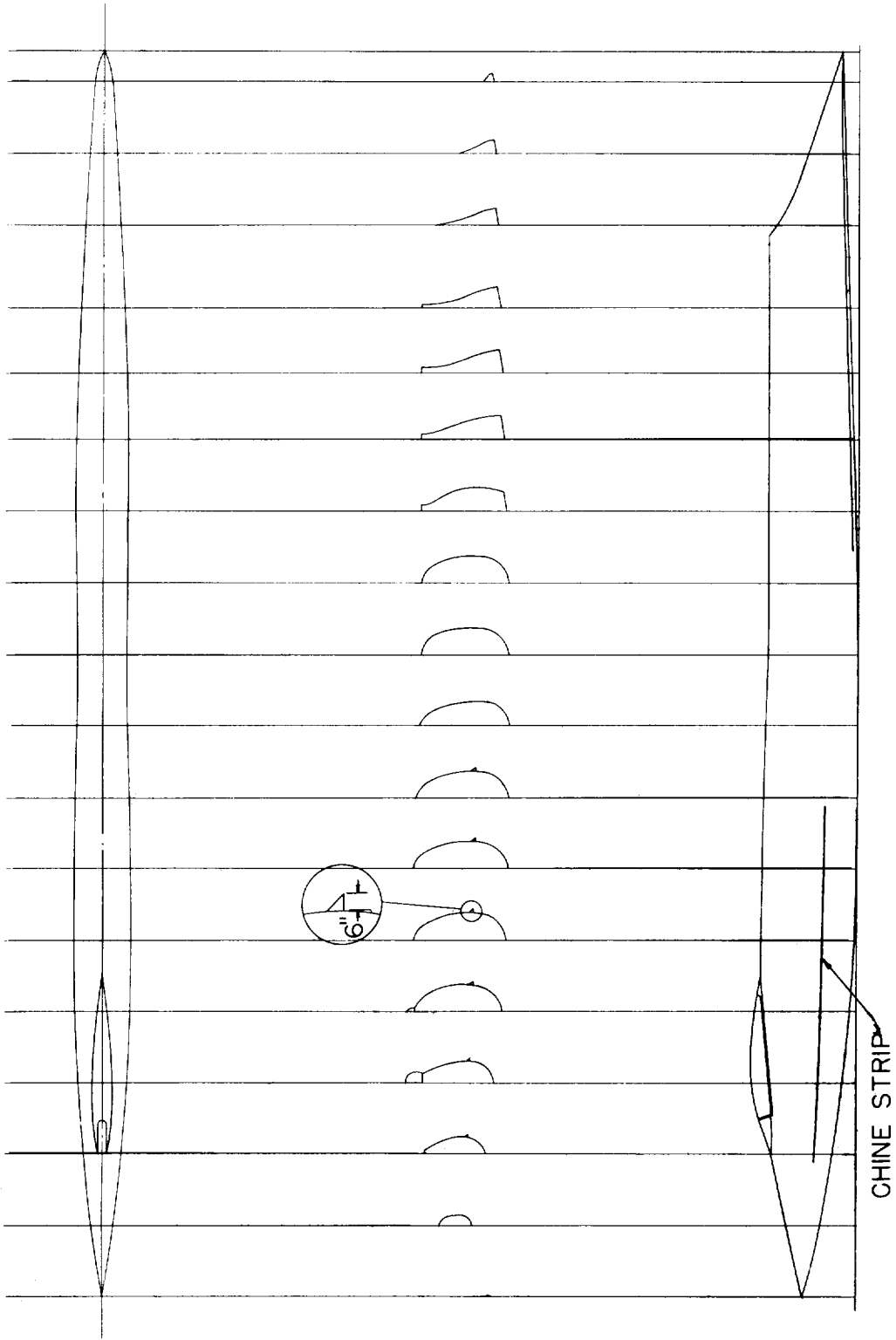
Figure 3.- Layout of fuselage lines.
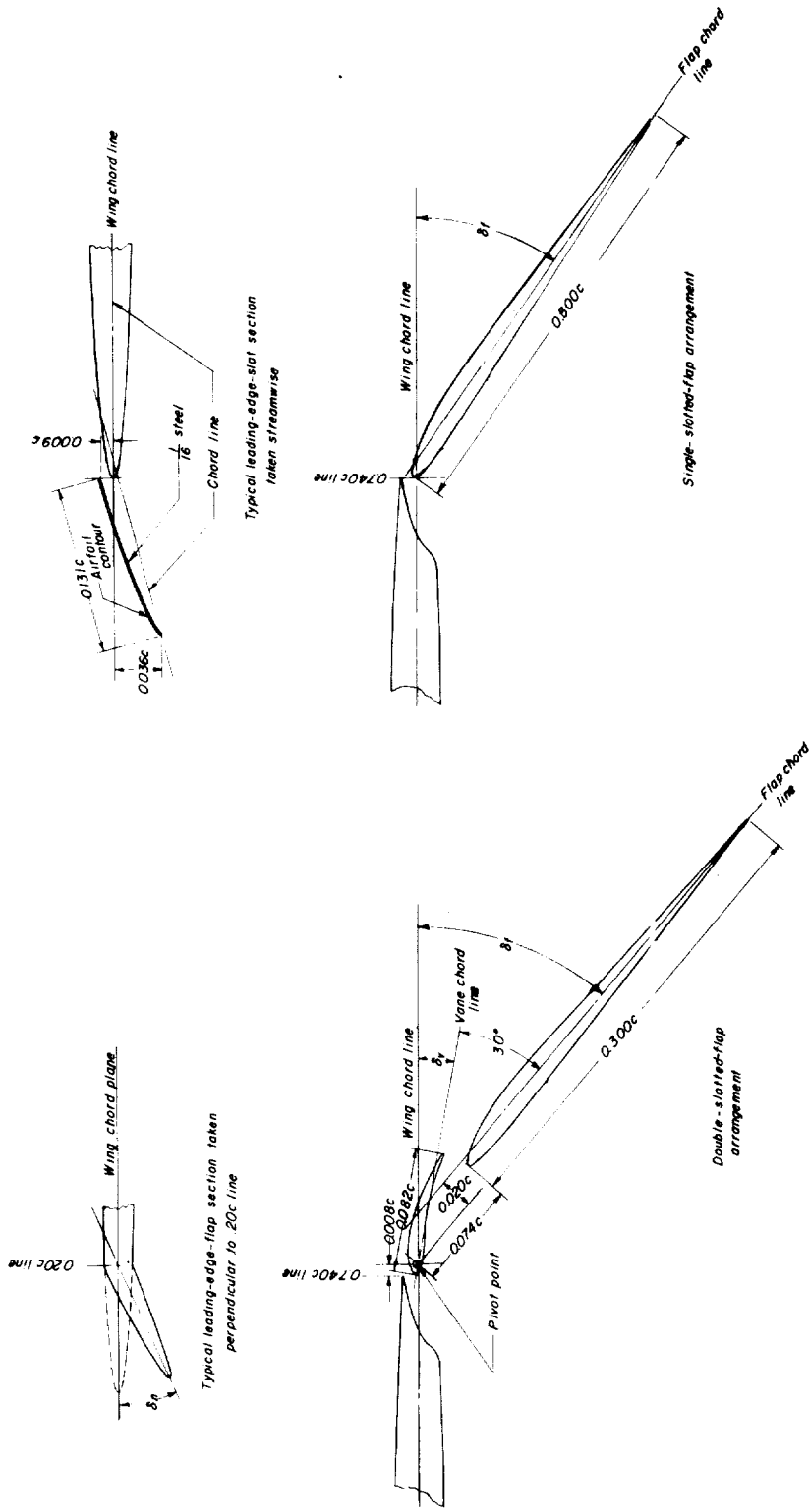
Figure 4.- Details of leading-edge flap, leading-edge slat, double slotted flap, and single slot- ted flap investigated on the model.
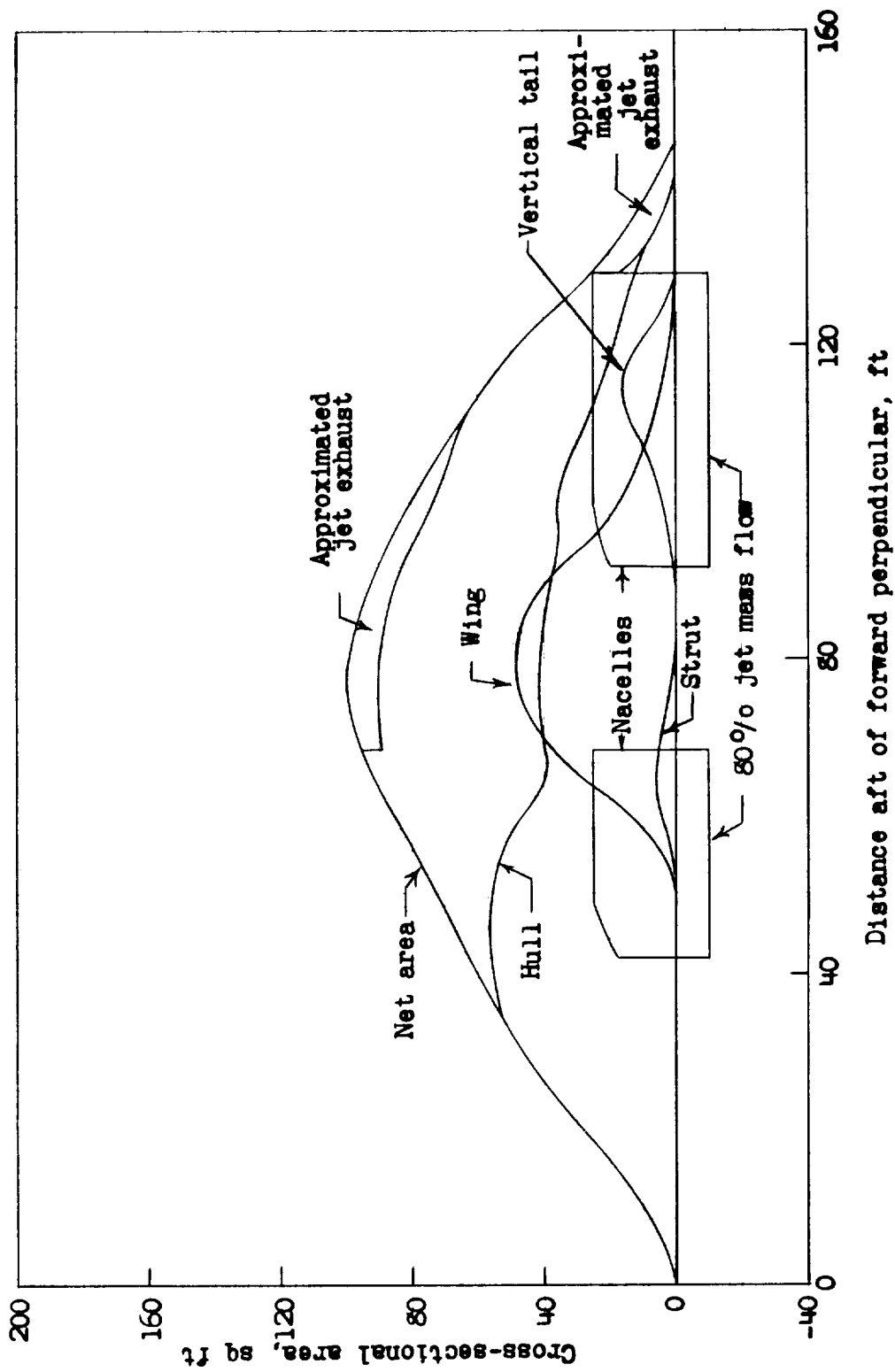
Figure 5.- Cross-sectional-area curves. M = 1.4.

BASELINE

A ←

A ←

440'

10.8'

5.0'

22.5'

21.5'

(a) Basic hydro-ski.

ASSUMED RETRACTED
POSITION

6.0'

2.0'

10°

SECTION A-A

10.8'

5.7'

5.0'

A ←

BASELINE

A ←
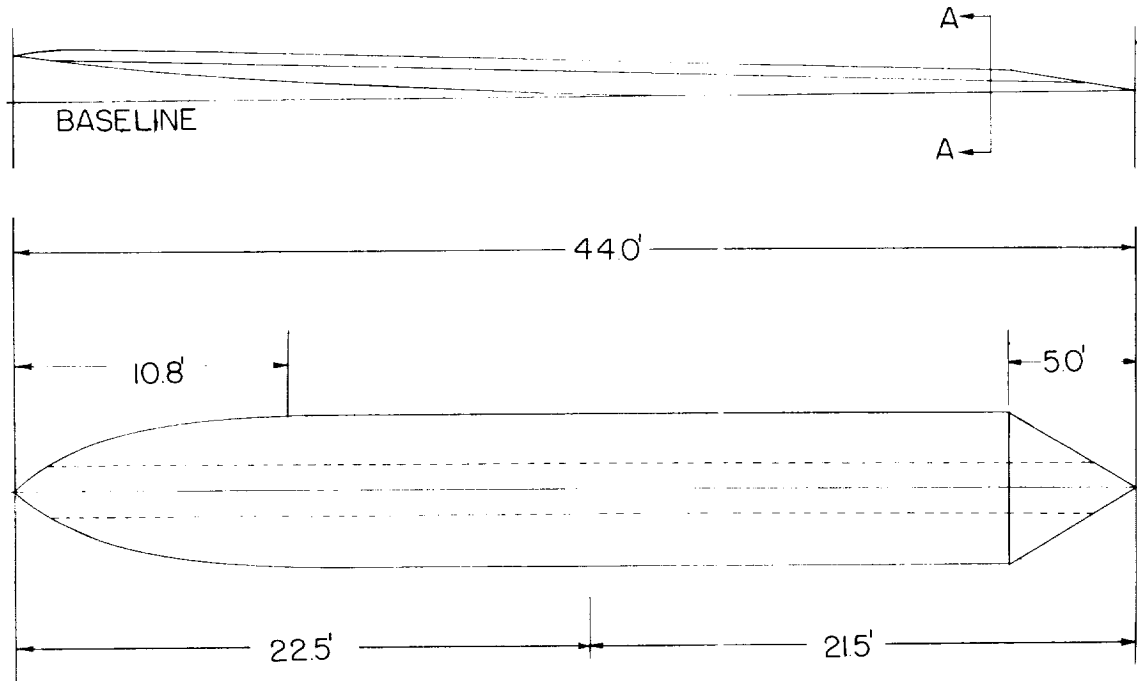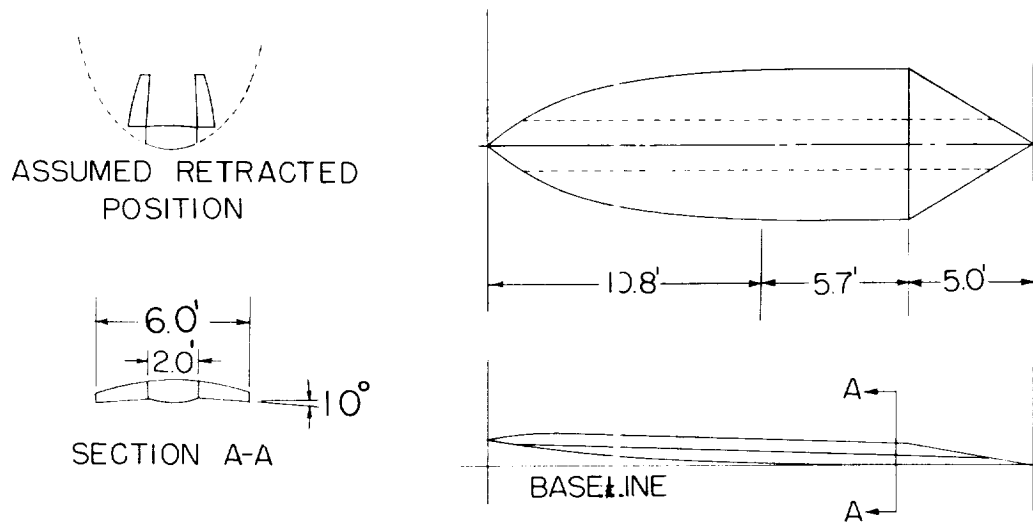
(b) Short hydro-ski.

Figure 6.- Layout of basic and short hydro-skis.
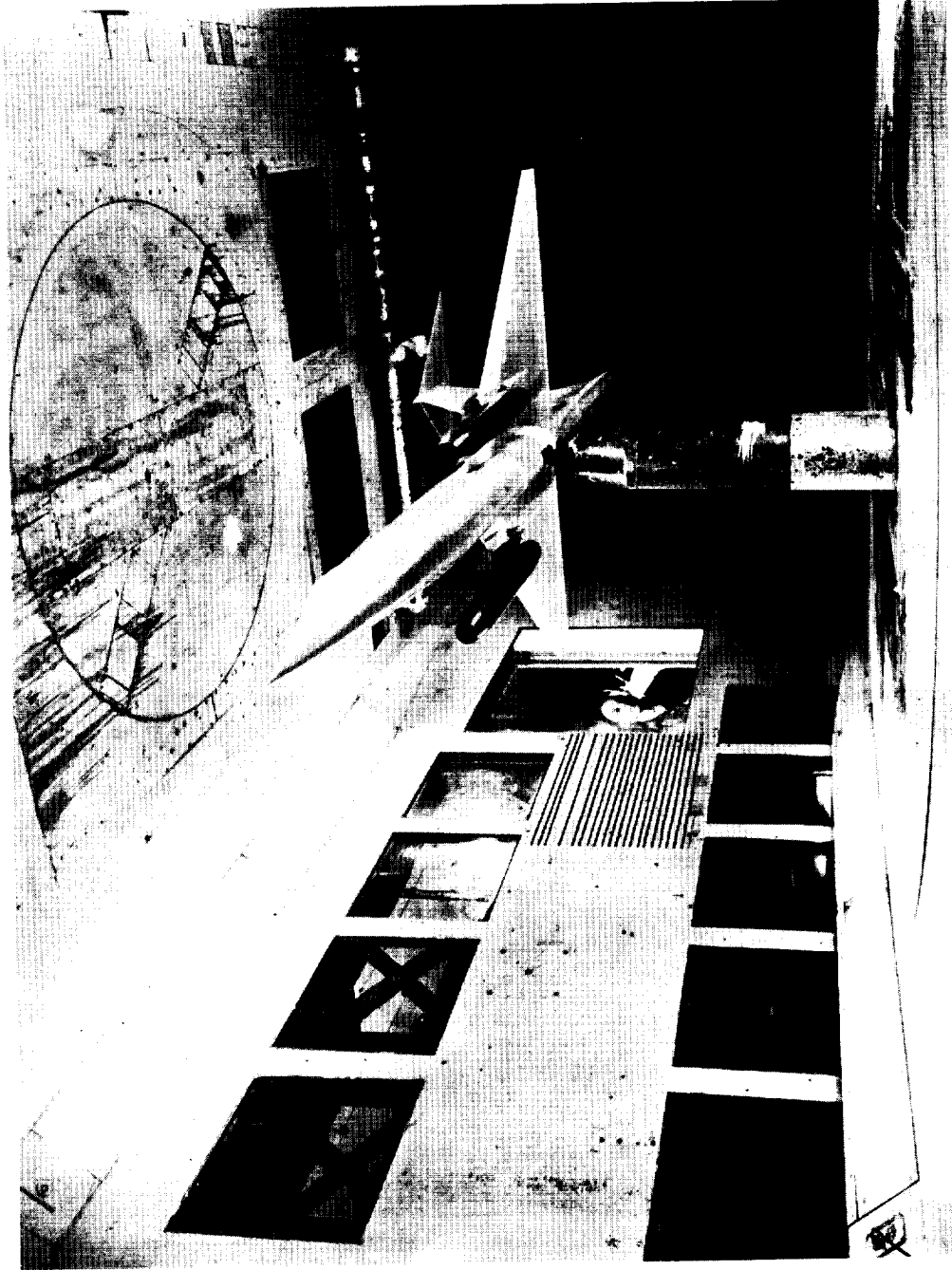
L-93243

Figure 7.- Setup of $\frac{1}{15}$-size model in the Langley 300-MPH 7- by 10-foot tunnel.
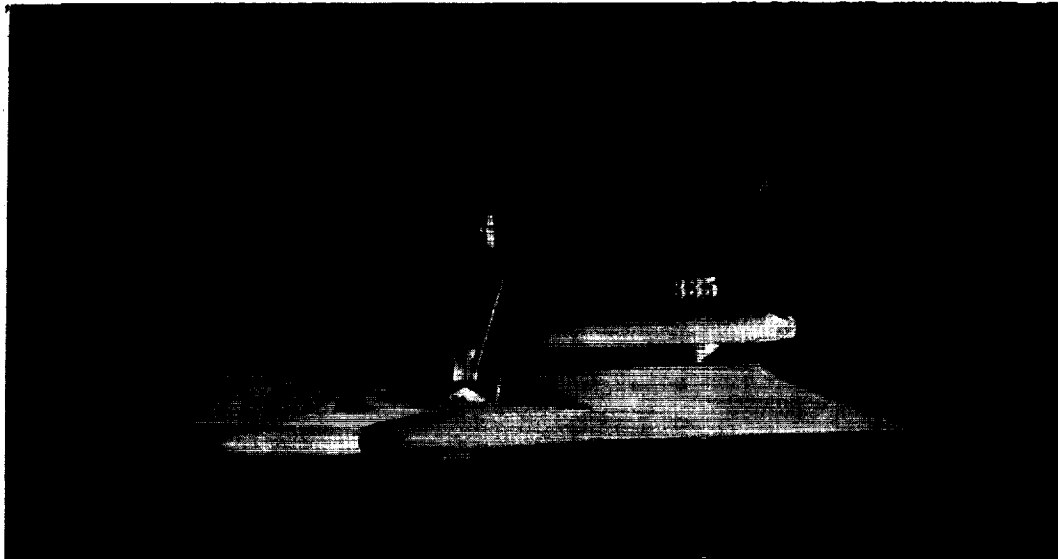
L-92934
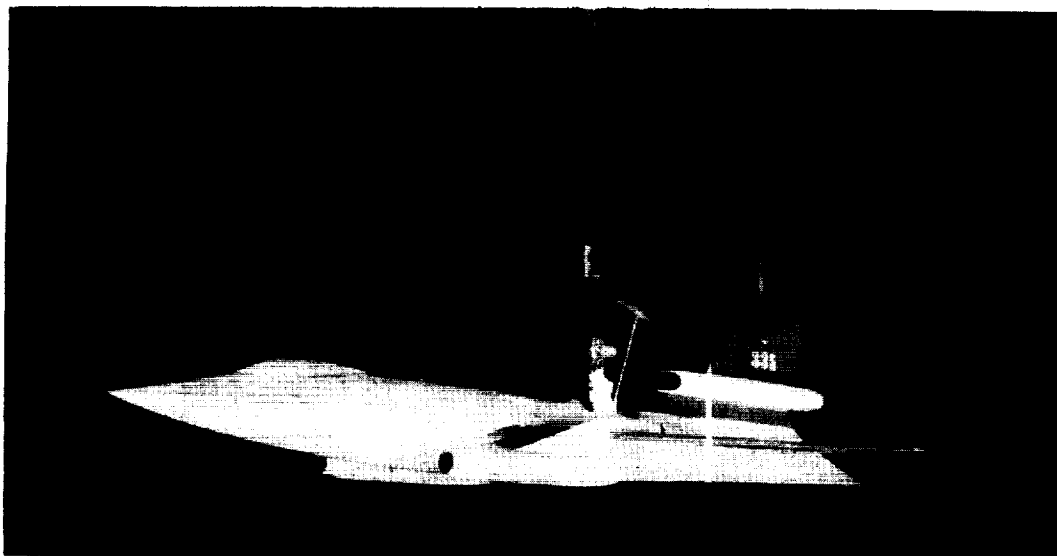
L-92933

Figure 8.- Photographs of $\frac{1}{15}$-size dynamic model tested in the Langley tank no. 1.
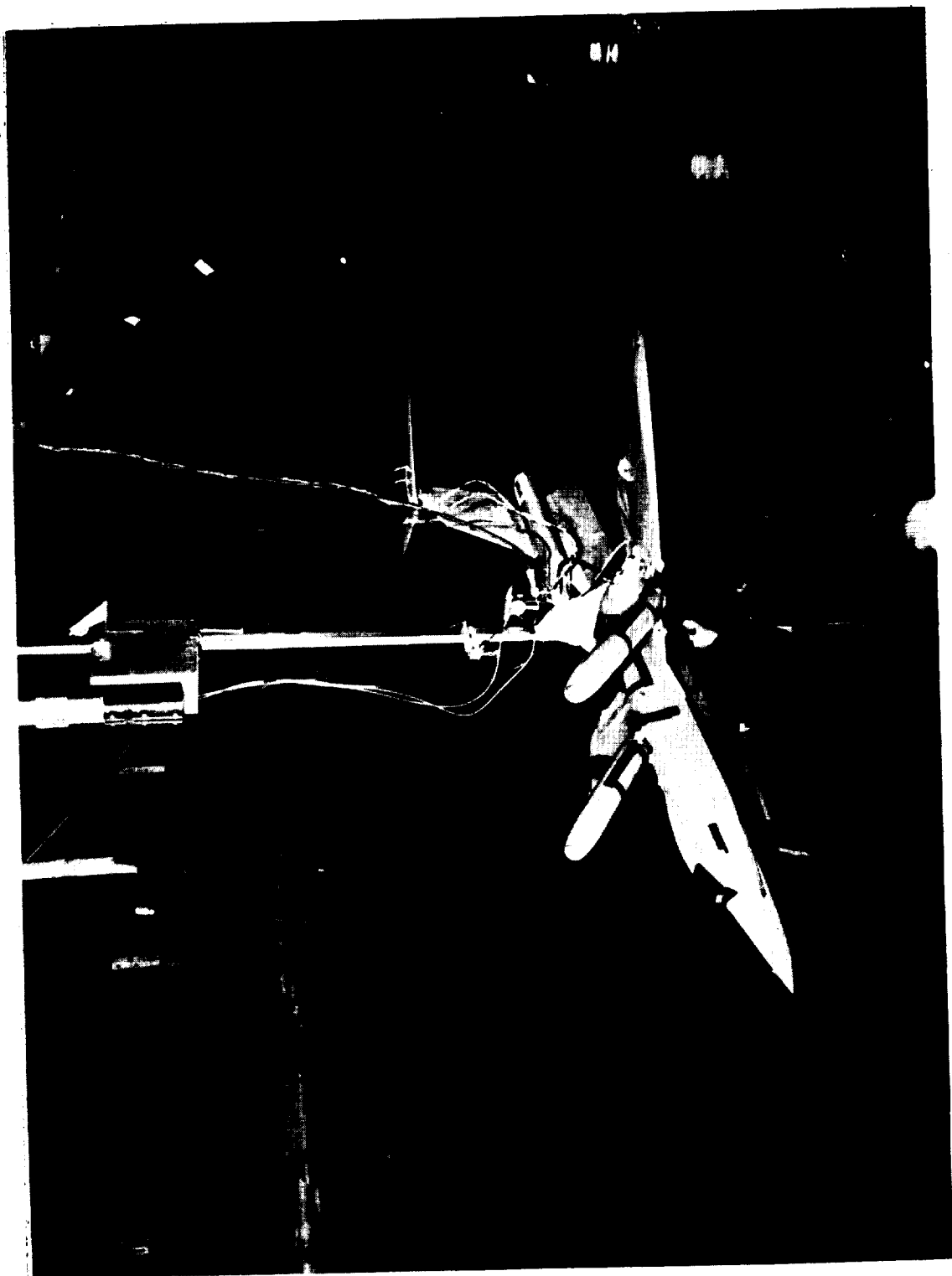
Figure 9.- Setup of model on towing apparatus.   L-58-2517
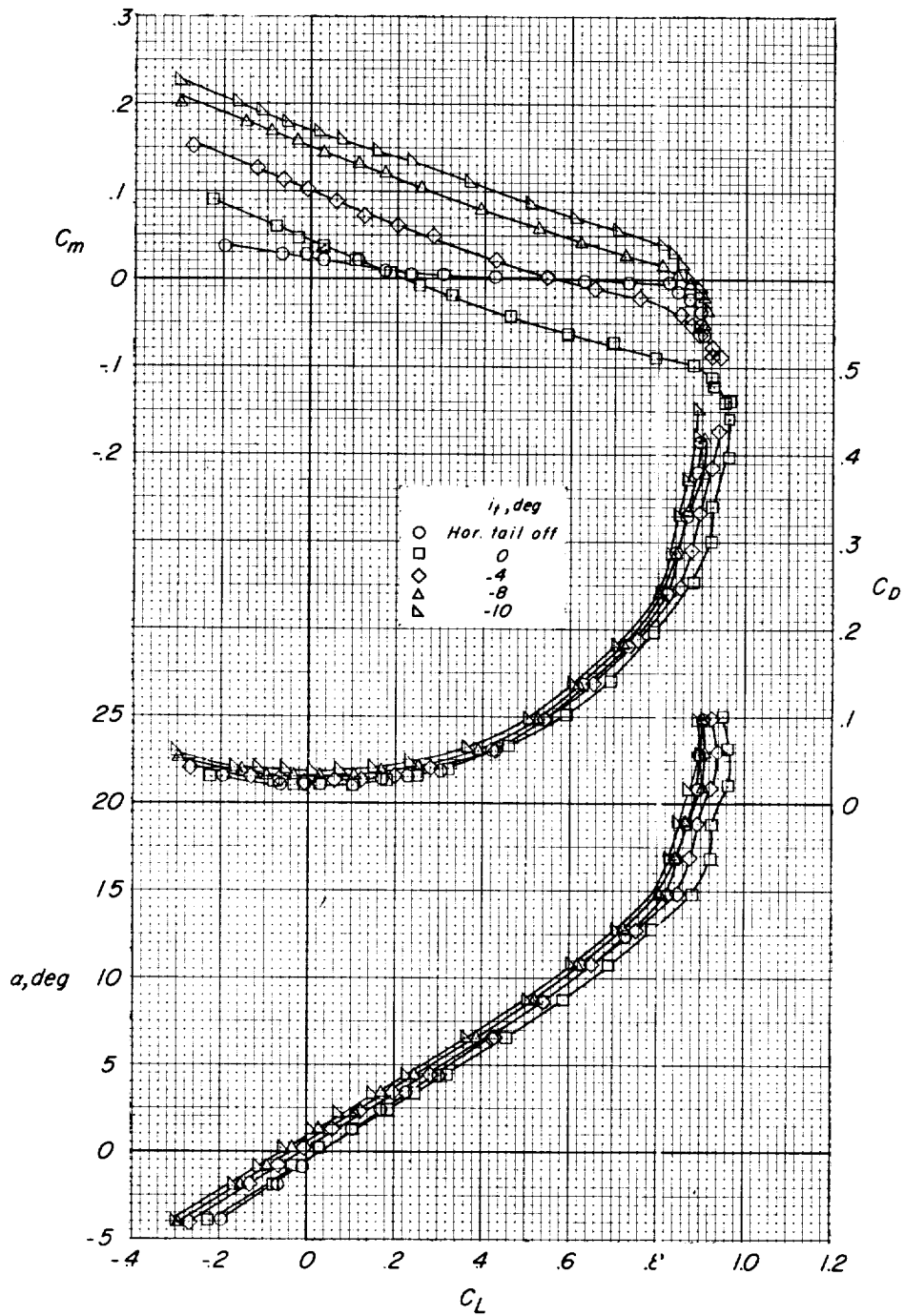
Figure 10.- Effect of horizontal-tail incidence on static longitudinal
aerodynamic characteristics of model. $\beta = 0^\circ$; $\delta_f = 0^\circ$; $\delta_n = 0^\circ$;
wing nacelle at 0°; tanks off; $q \approx 45$ lb/sq ft.

Z
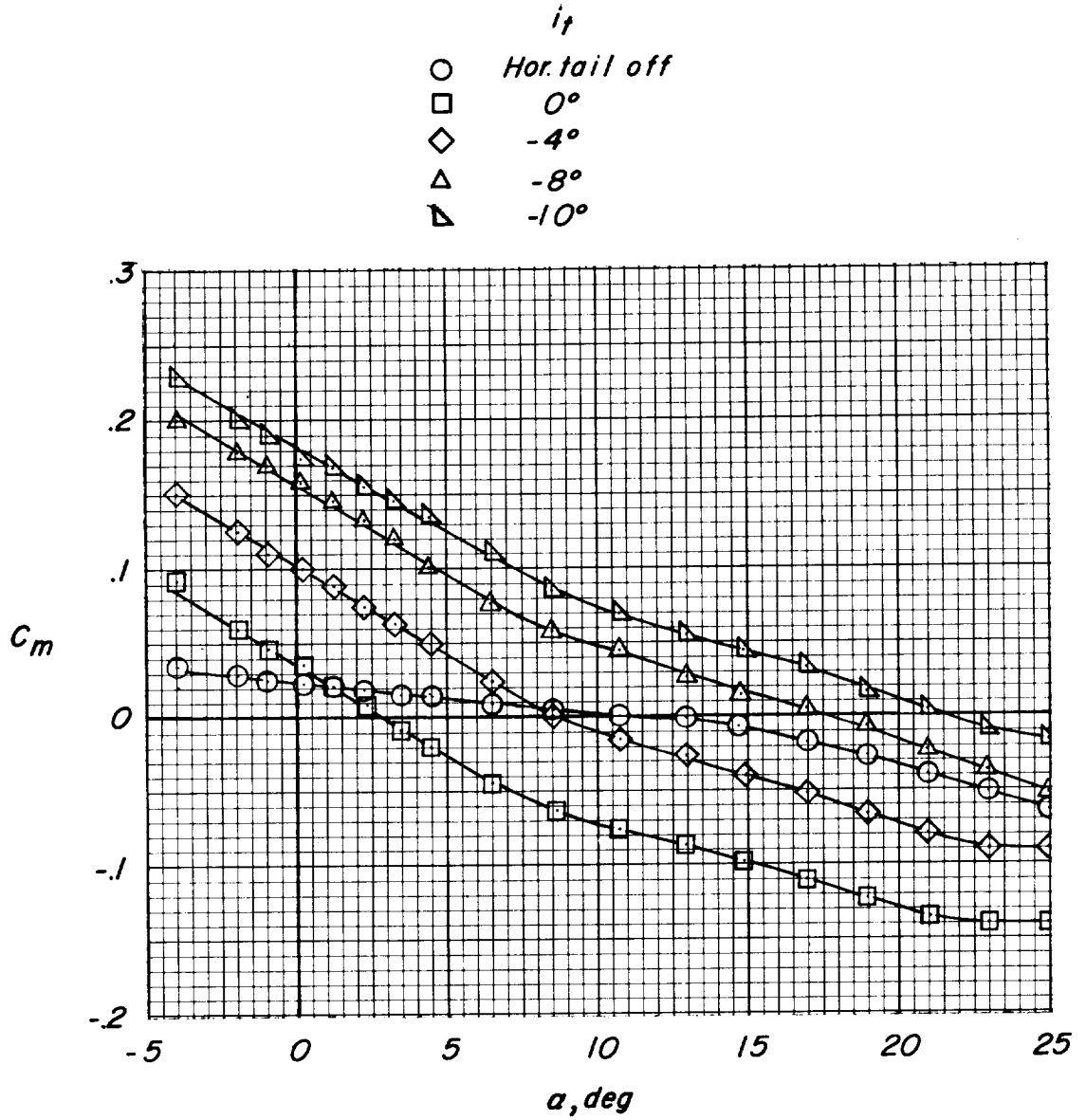
Figure 10.- Concluded.
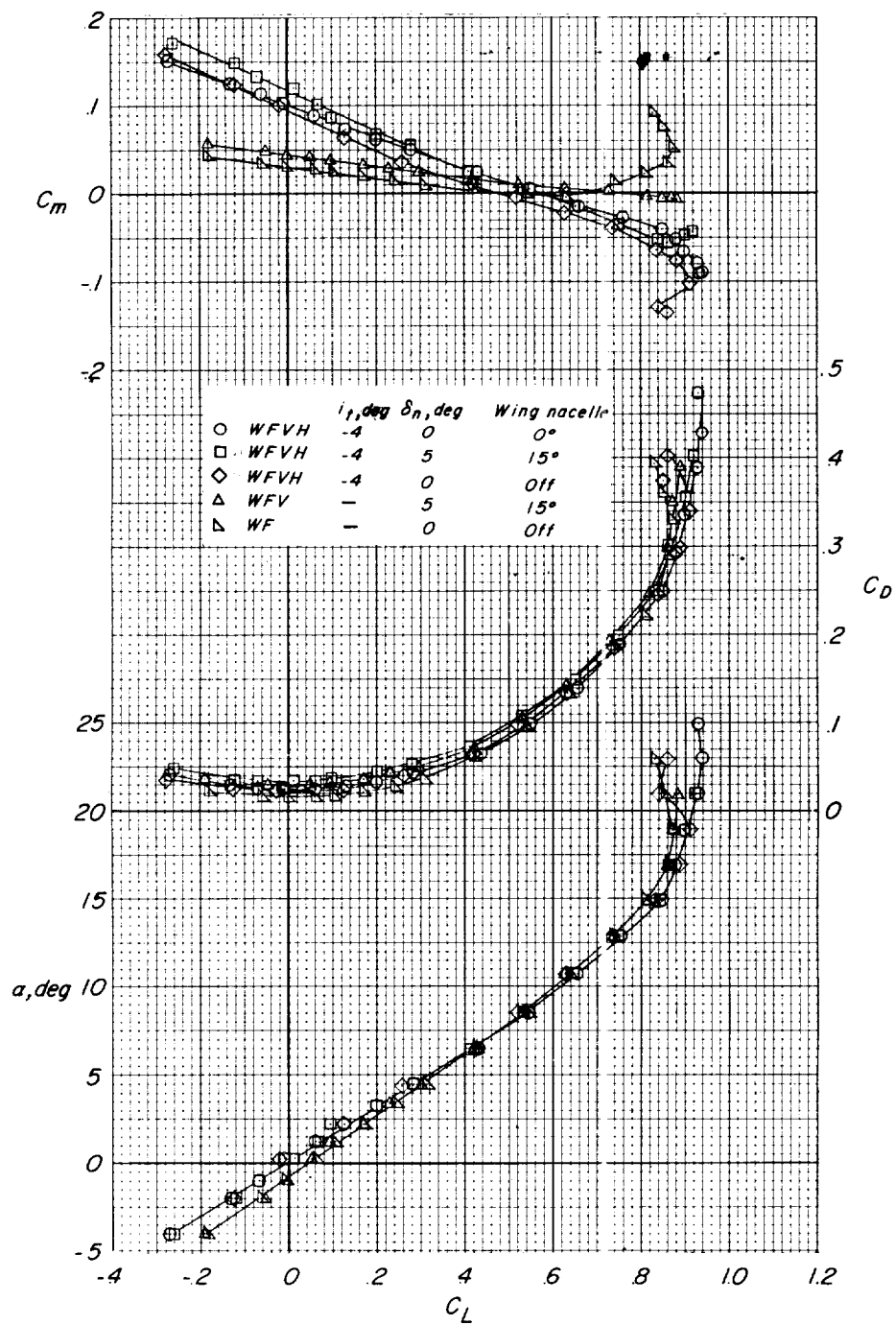
Figure 11.- Effect of leading-edge-flap deflection and wing-nacelle position on static longitudinal aerodynamic characteristics of model. β = 0°; δ_f = 0°; tanks off; q ≈ 45 lb/sq f:.

		i_t, deg	δ_n, deg	Wing nacelles
○	WFVH	-4	0	0°
□	WFVH	-4	5	15°
◇	WFVH	-4	0	Off
△	WFV	—	5	15°
◁	WF	—	0	Off

Figure 11.- Concluded.

36

	a,deg	i_t,deg	δ_n,deg	Wing nacelle
○	0.2	0	0	0°
□	8.6	-4	0	0°
◇	16.9	-8	0	0°
△	8.6	-4	5	15°
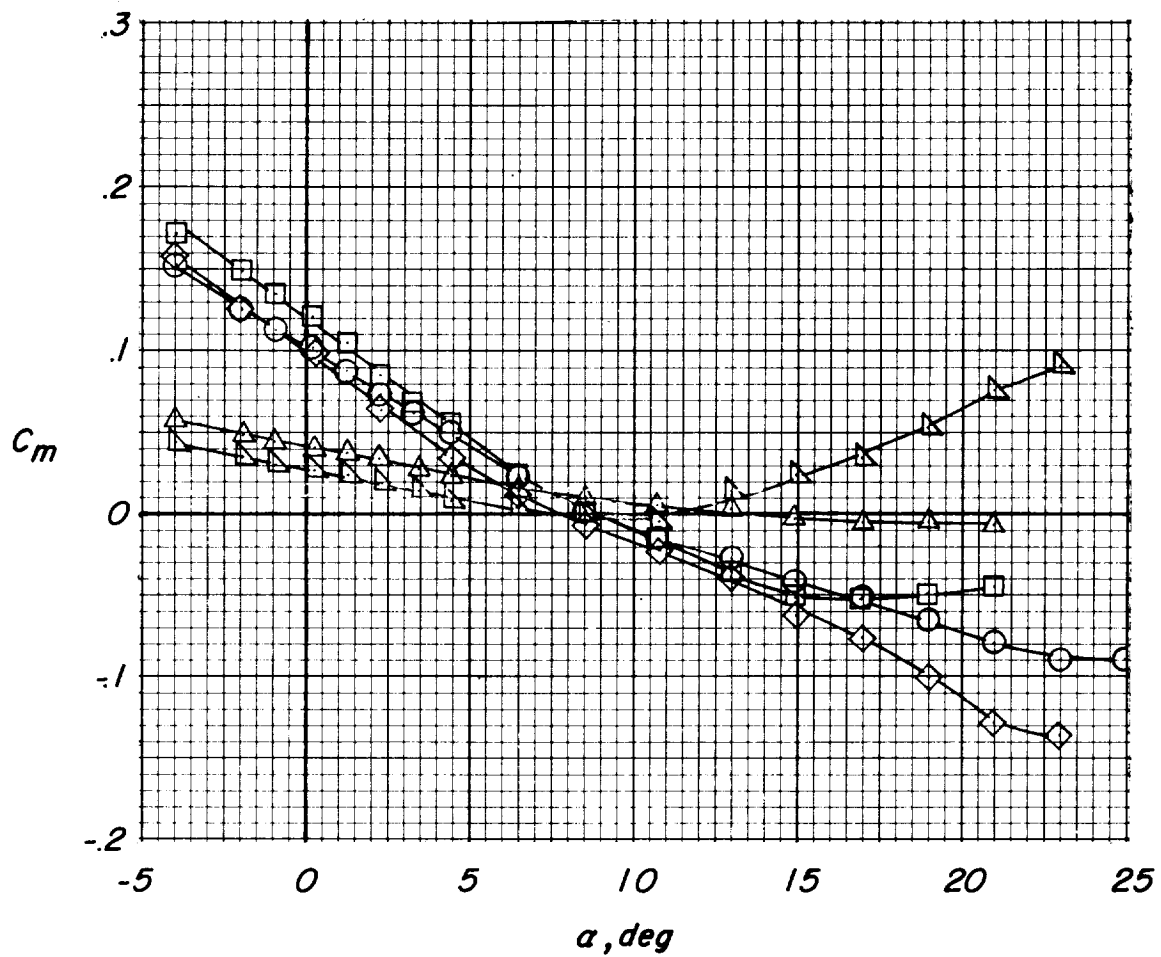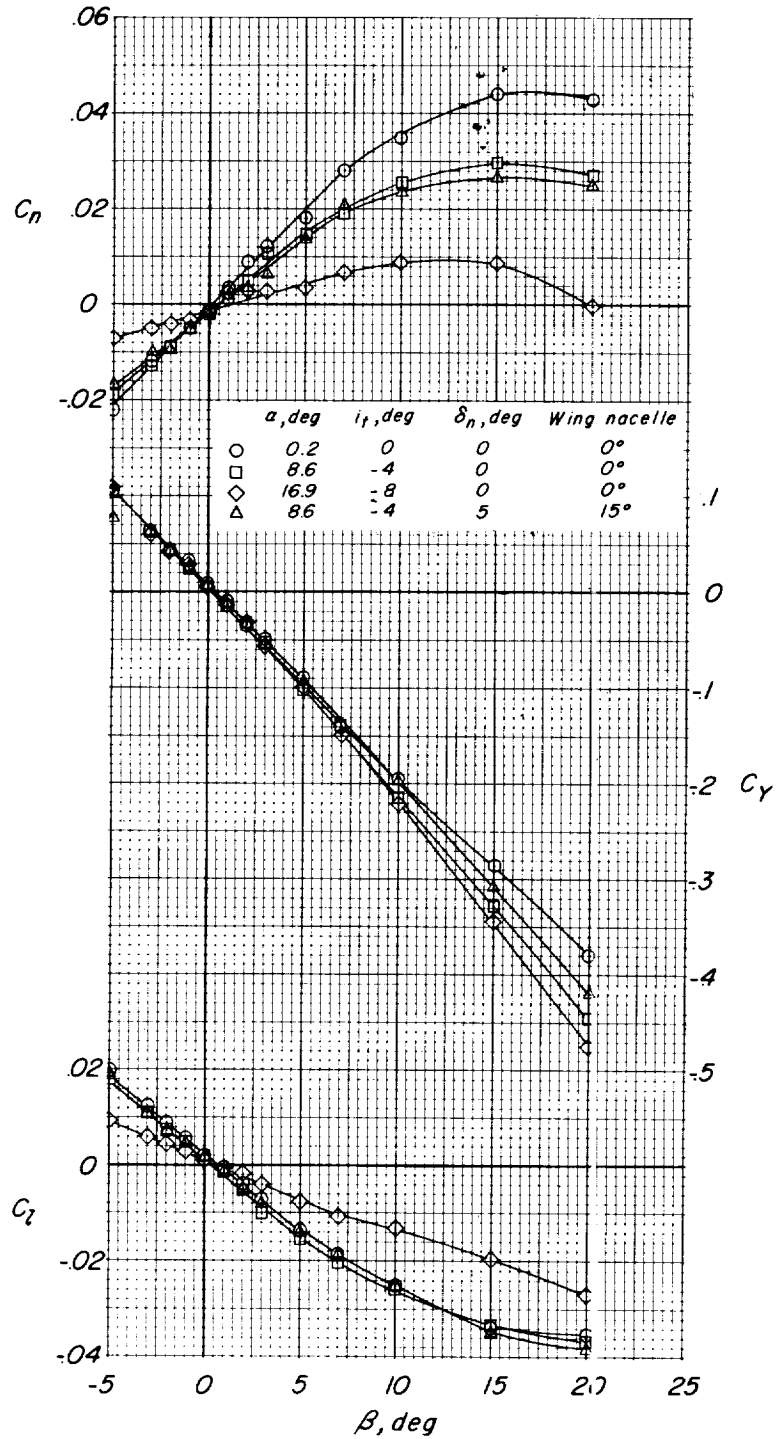
Figure 12.- Effect of angle of attack on static lateral aerodynamic characteristics of model. δ_f = 0°; tanks off; q ≈ 28 lb/sq ft.
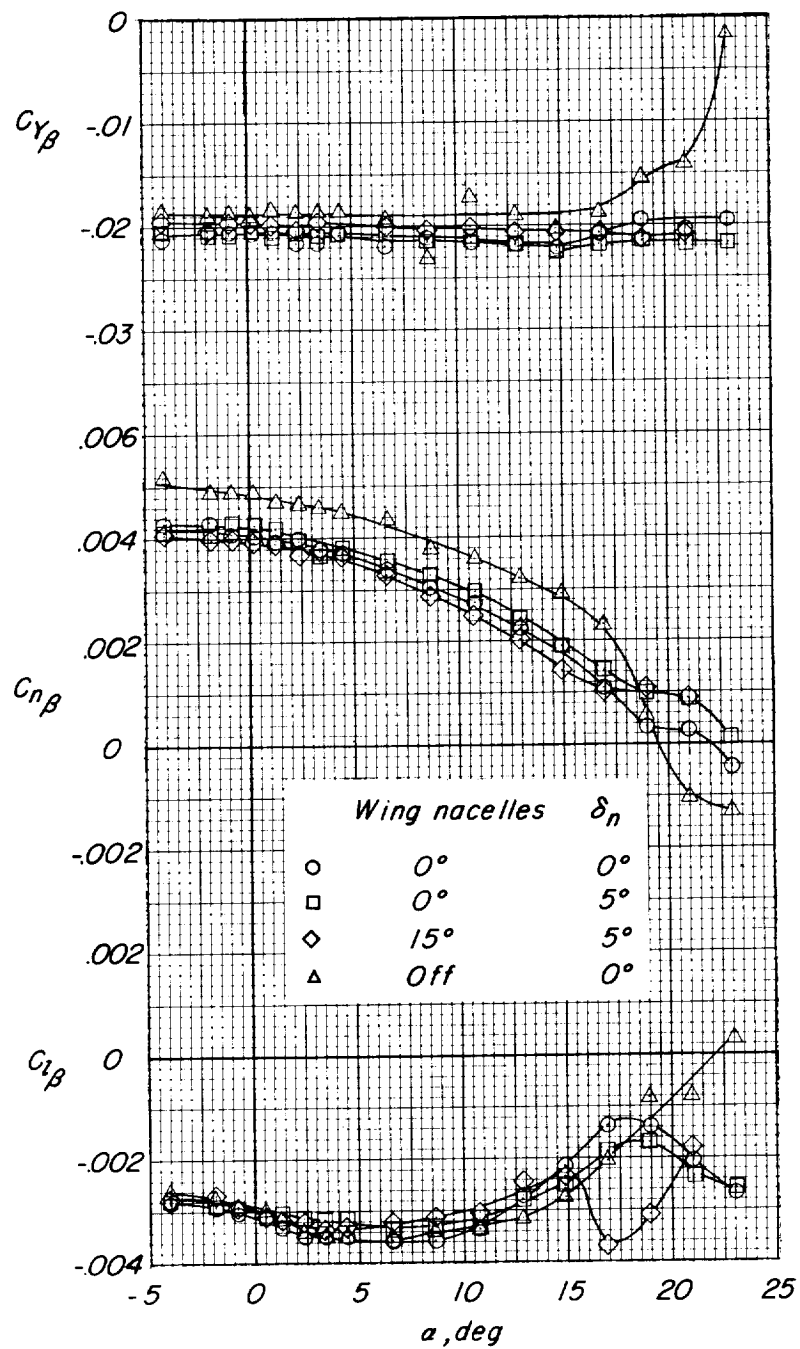
Figure 13.- Effect of leading-edge-flap deflection and wing-nacelle position on static lateral stability derivatives of model. $\delta_f = 0^\circ$; $i_t = -4^\circ$; tanks off; $q \approx 45$ lb/sq ft; $\beta = \pm 4^\circ$.
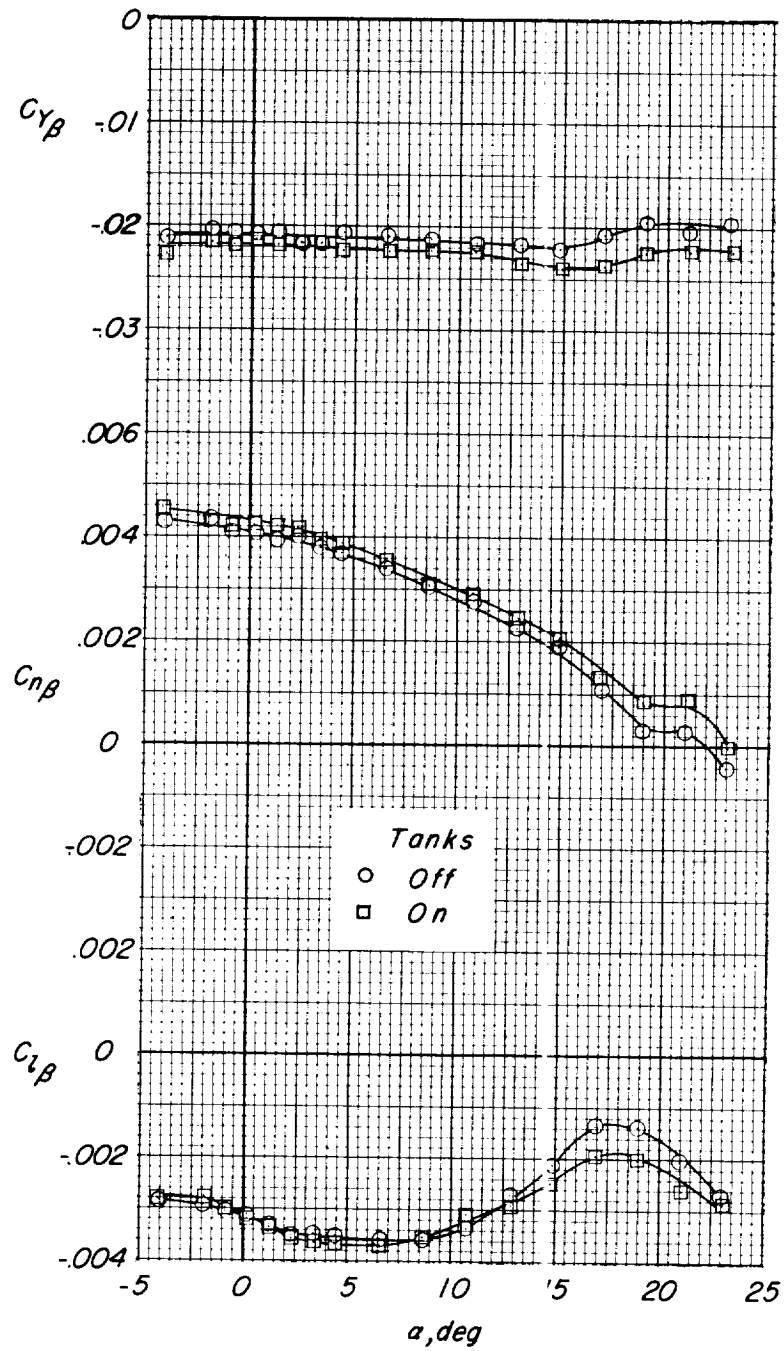
Figure 14.- Effect of wing tanks on static lateral stability derivatives of model. $\delta_f = 0°$; $i_t = -4°$; $\delta_n = 0°$; wing nacelles at $0°$; $q \approx 45$ lb/sq ft; $\beta = \pm 4°$.
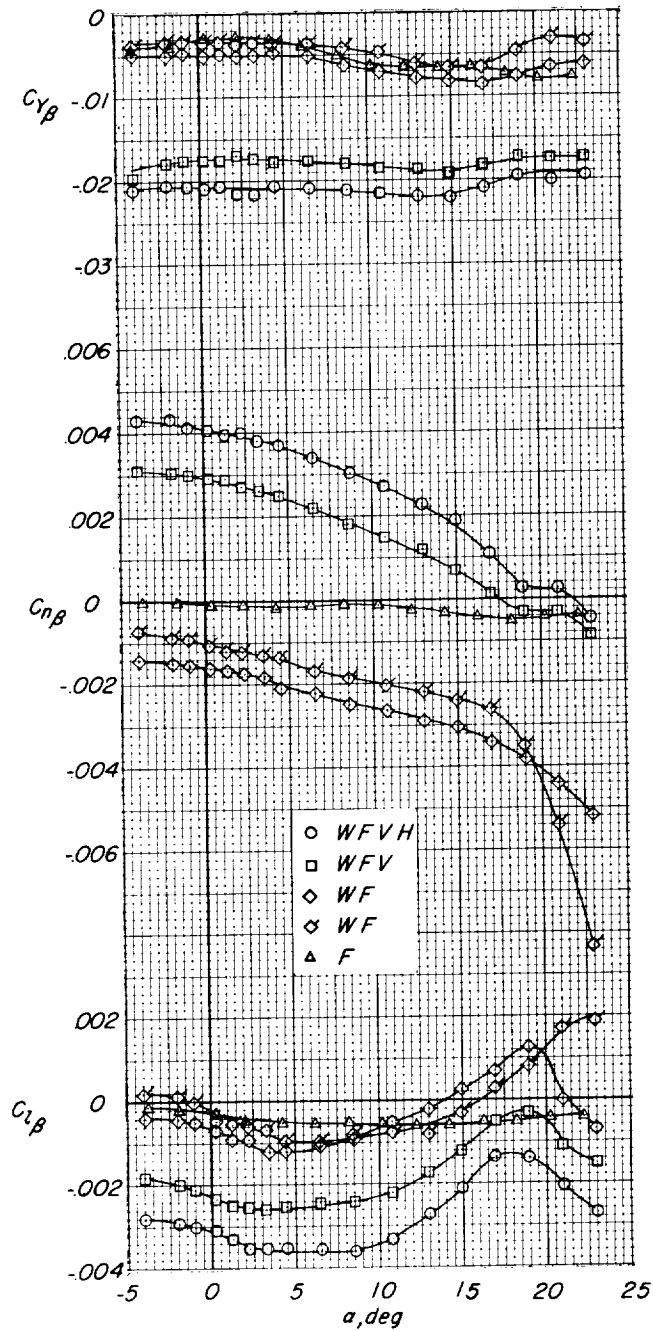
Figure 15.- Effect of model configuration on static lateral stability derivatives. $\delta_f = 0^\circ$; $i_t = -4^\circ$; $\delta_n = 0^\circ$; wing nacelles at 0°; $q \approx 45$ lb/sq ft; $\beta = \pm4^\circ$. Flagged symbols indicate wing nacelles off.
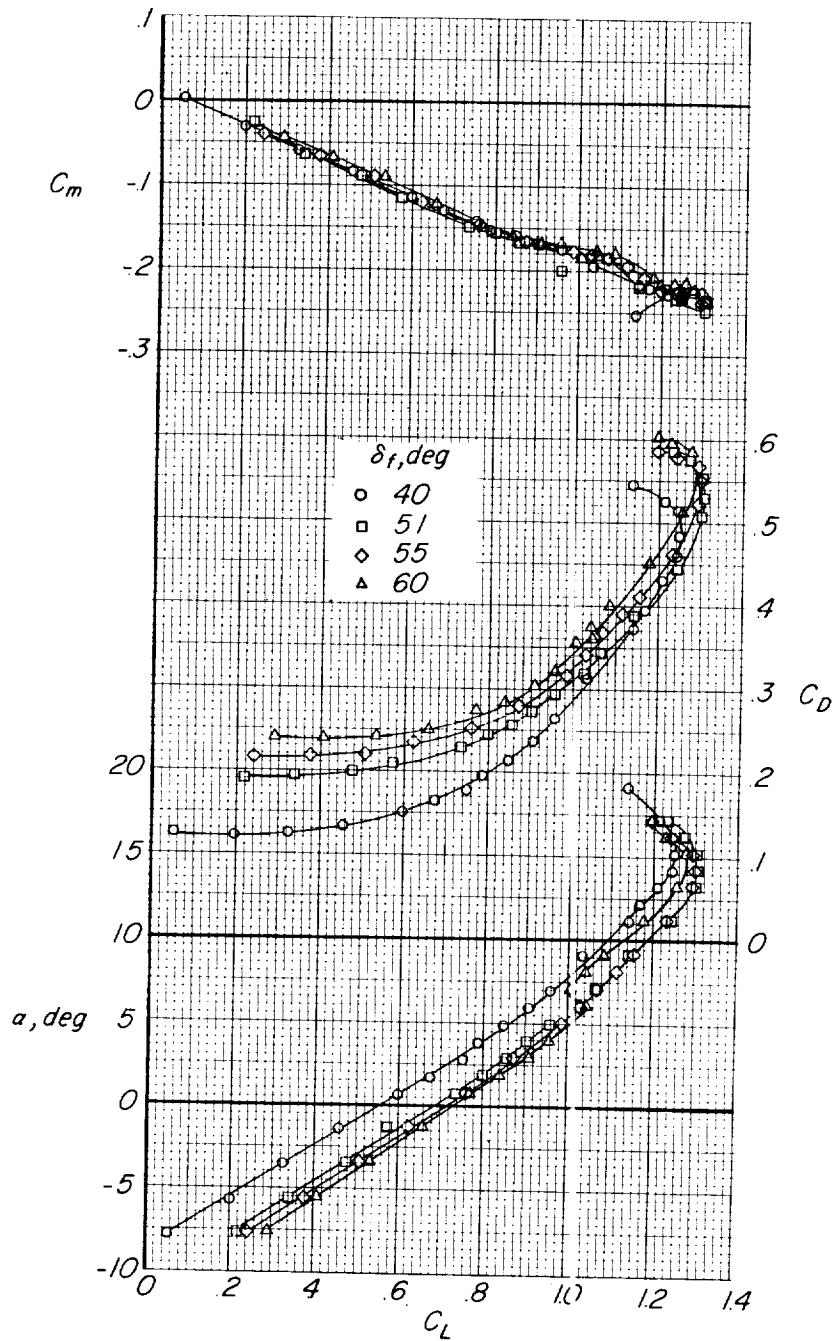
Figure 16.- Effect of short-span inboard double-slotted-flap deflection on static longitudinal aerodynamic characteristics of model. $i_t = 0°$; $\beta = 0°$; $\delta_n = 0°$; tanks off; wing nacelles off; $q \approx 28$ lb/sq ft; flap span from $0.074b/2$ to $0.397b/2$.
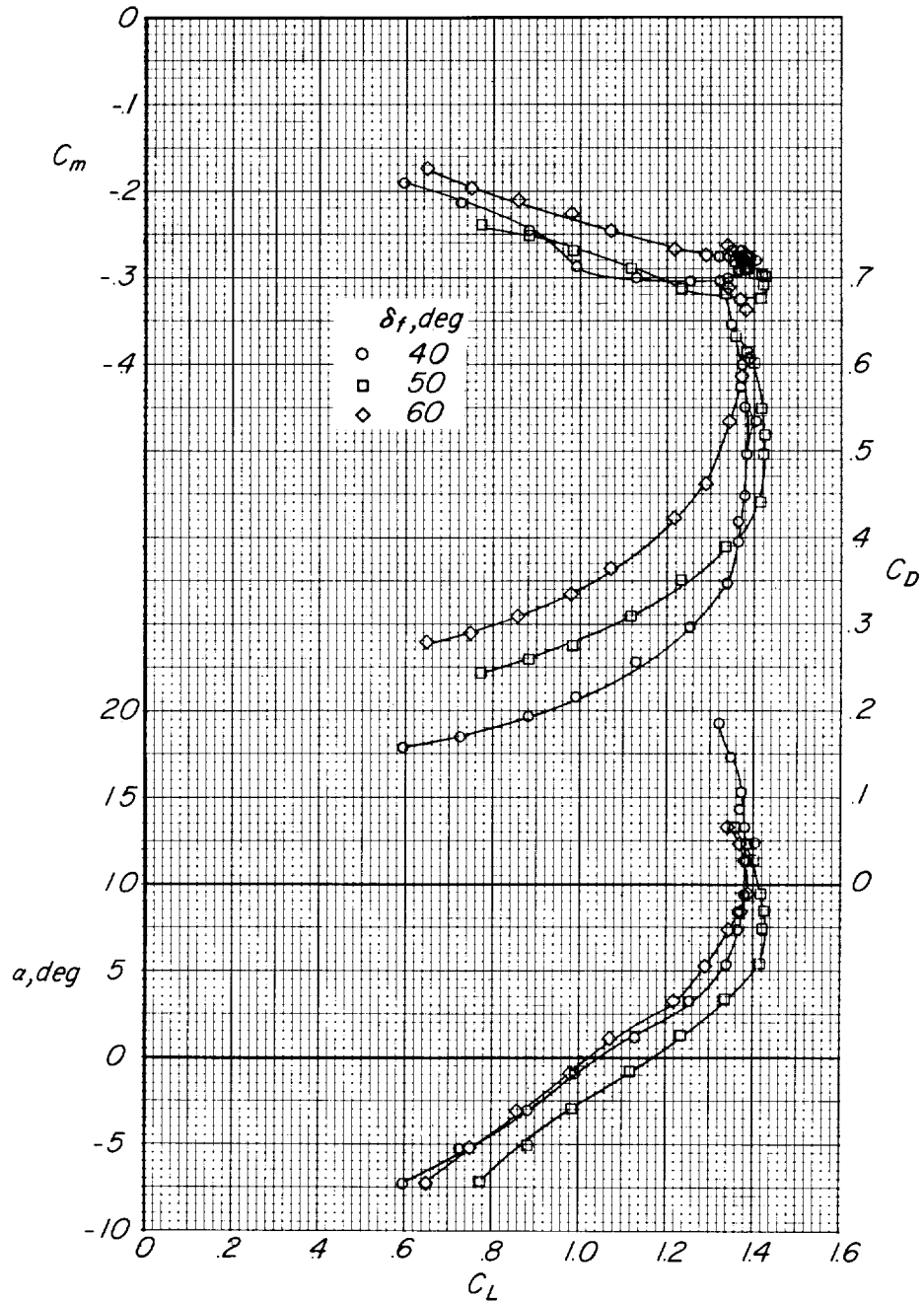
Figure 17.- Effect of medium-span inboard double-slotted-flap deflection
on static longitudinal aerodynamic characteristics of model.
$i_t = 0^0$; $\beta = 0^0$; $\delta_n = 0^0$; tanks off; wing nacelles at 0^0;
$q \approx 28$ lb/sq ft; flap span from $0.074b/2$ to $0.751b/2$.
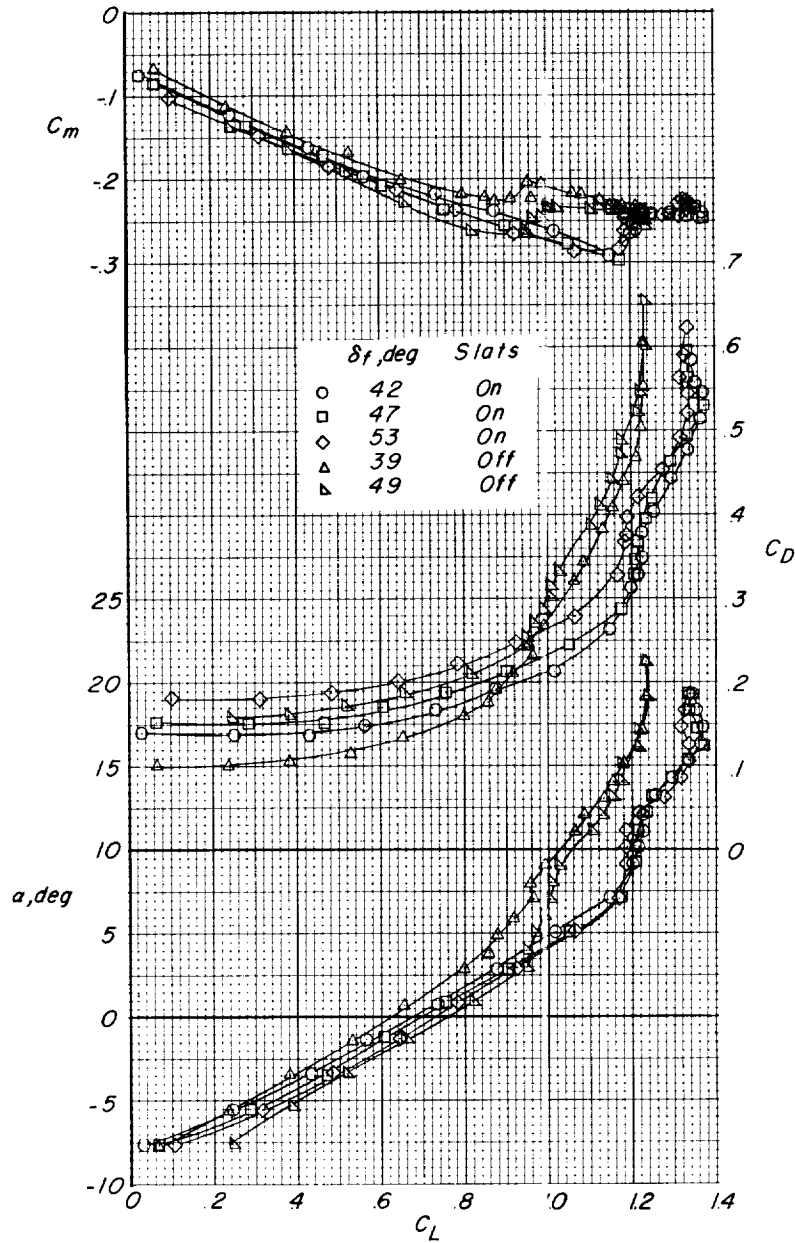
Figure 18.- Effect of medium-span outboard louble-slotted-flap deflection, with and without slats, on static longitudinal aerodynamic characteristics of model. $i_t = 0°$; $\beta = 0°$; $\delta_n = 0°$; tanks off; wing nacelles at $0°$; $q \approx 28$ lb/sq ft; flap span from $0.397b/2$ to $1.000b/2$.
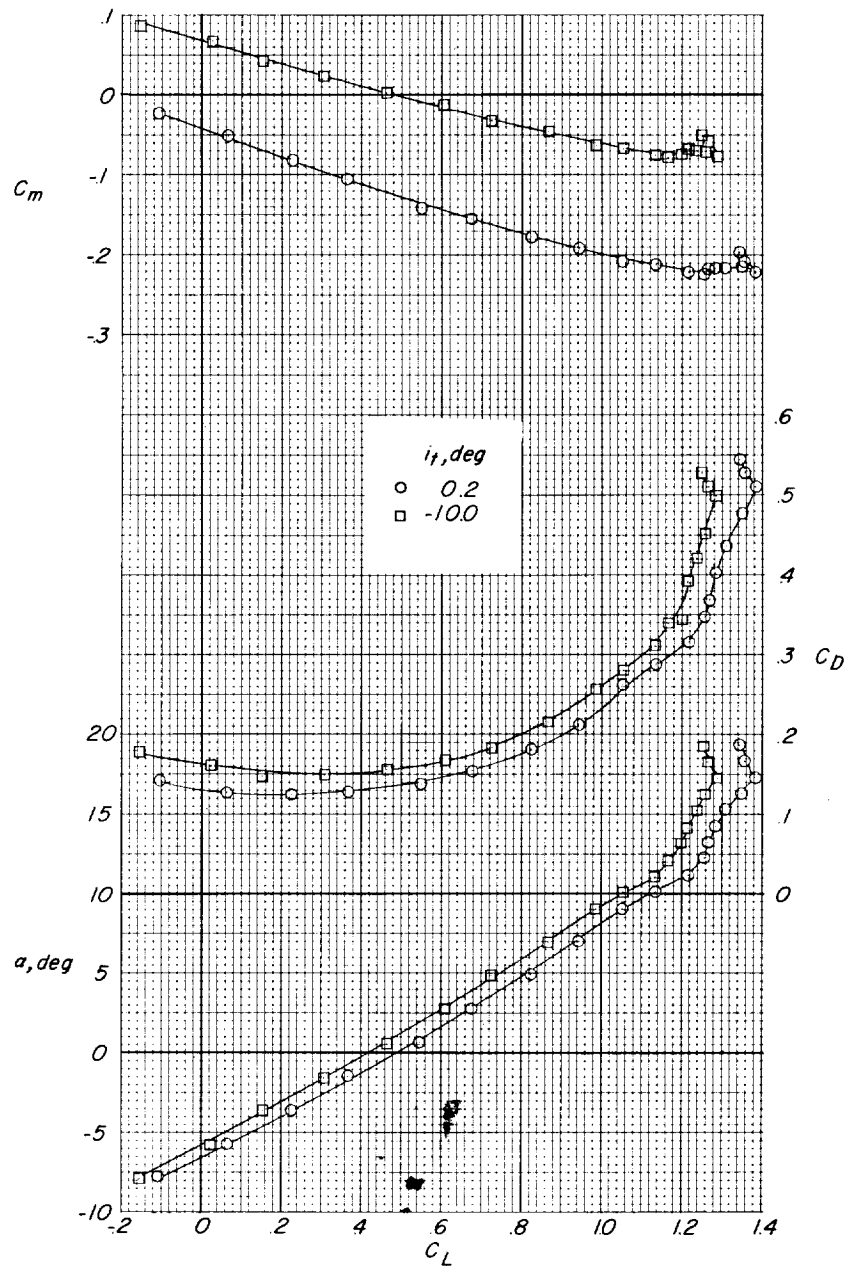
Figure 19.- Effect of horizontal-tail incidence on static longitudinal aerodynamic characteristics of model equipped with midspan double slotted flaps. $\beta = 0°$; $\delta_n = 0°$; wing nacelles at $0°$; wing slats on; $q \approx 28$ lb/sq ft; $\delta_f = 42°$; flap span from $0.397b/2$ to $0.751b/2$.
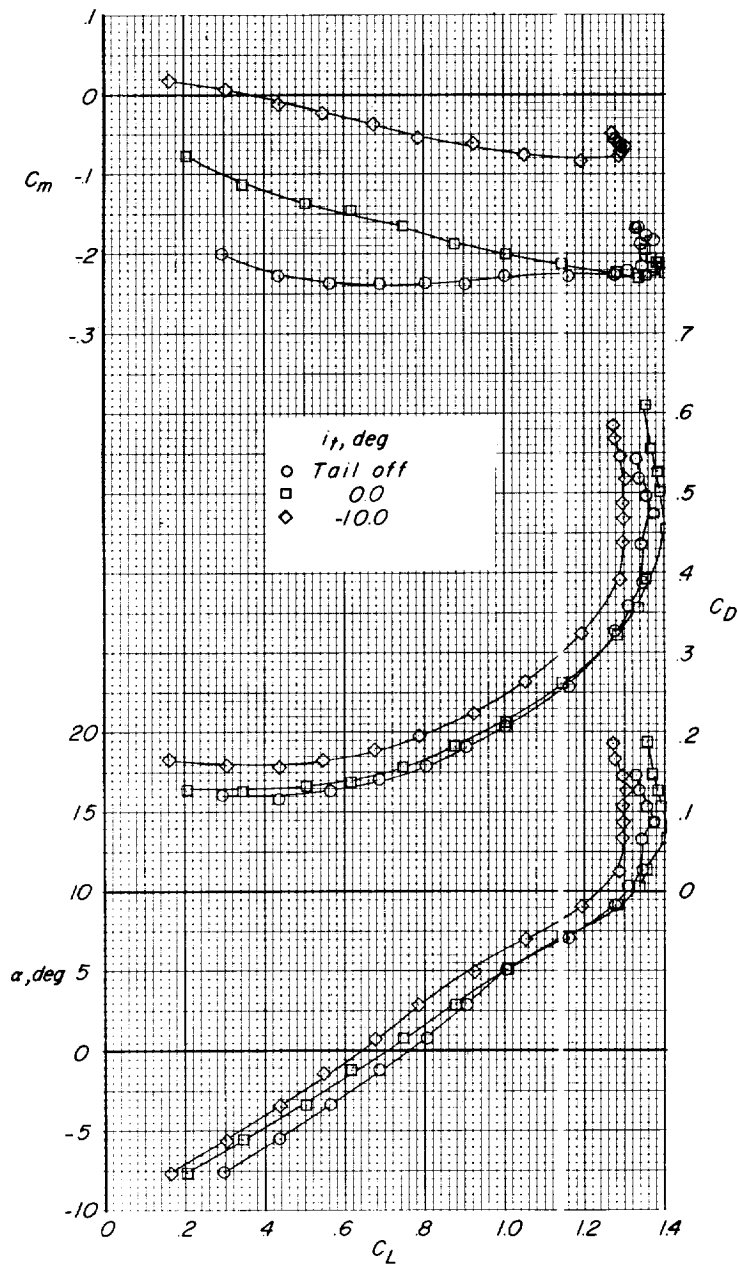
Figure 20.- Effect of horizontal-tail incidence on static longitudinal
aerodynamic characteristics of model equipped with full-span single
slotted flaps. $\beta = 0°$; $\delta_n = 0°$; wing nacelles at $0°$; wing leading-
edge slats on; $q \approx 28$ lb/sq ft; $\delta_f = 31°$; flap span from $0.074b/2$
to $1.000b/2$.
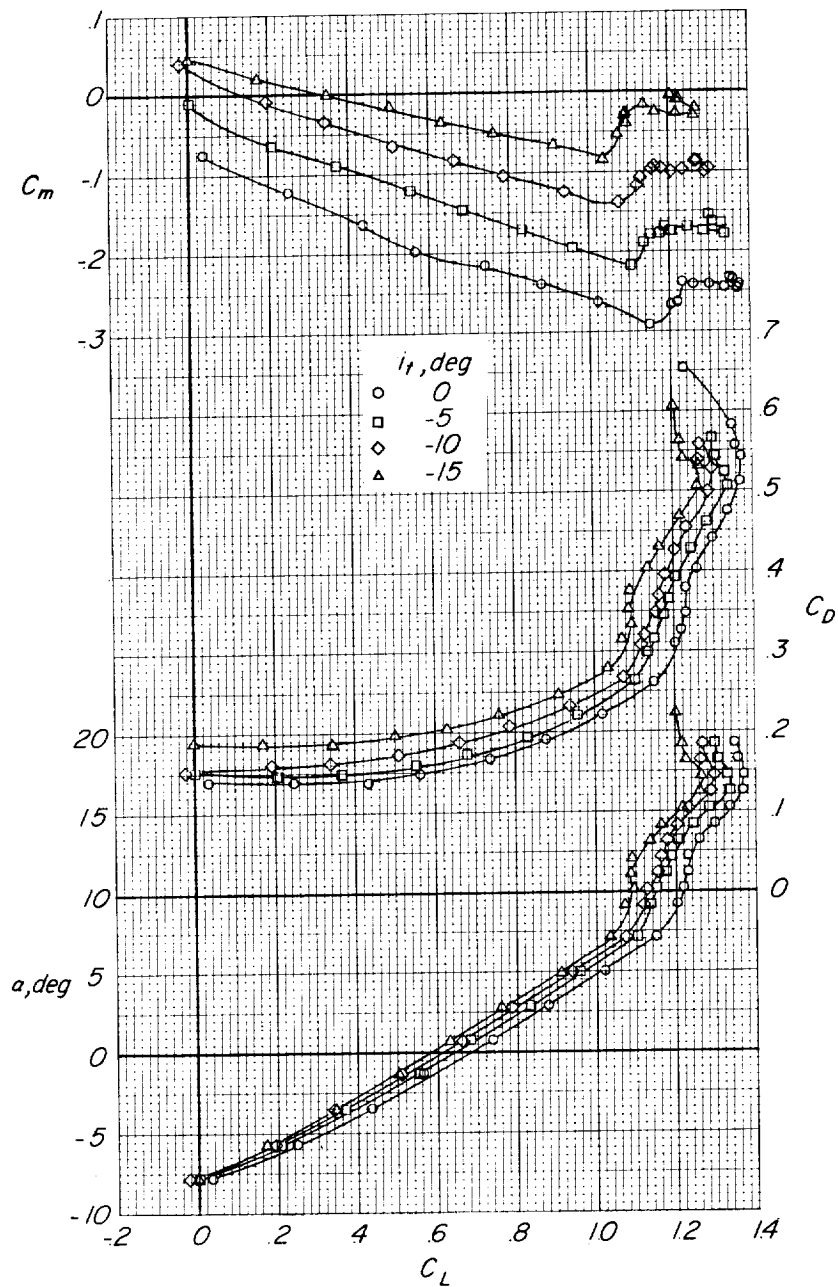
Figure 21.- Effect of horizontal-tail incidence on static longitudinal aerodynamic characteristics of model equipped with medium-span outboard double slotted flaps. $\delta_f = 42°$; $\beta = 0°$; $\delta_n = 0°$; tanks off; wing nacelles at $0°$; wing slats on; $q \approx 28$ lb/sq ft; flap span from 0.397b/2 to 1.000b/2.
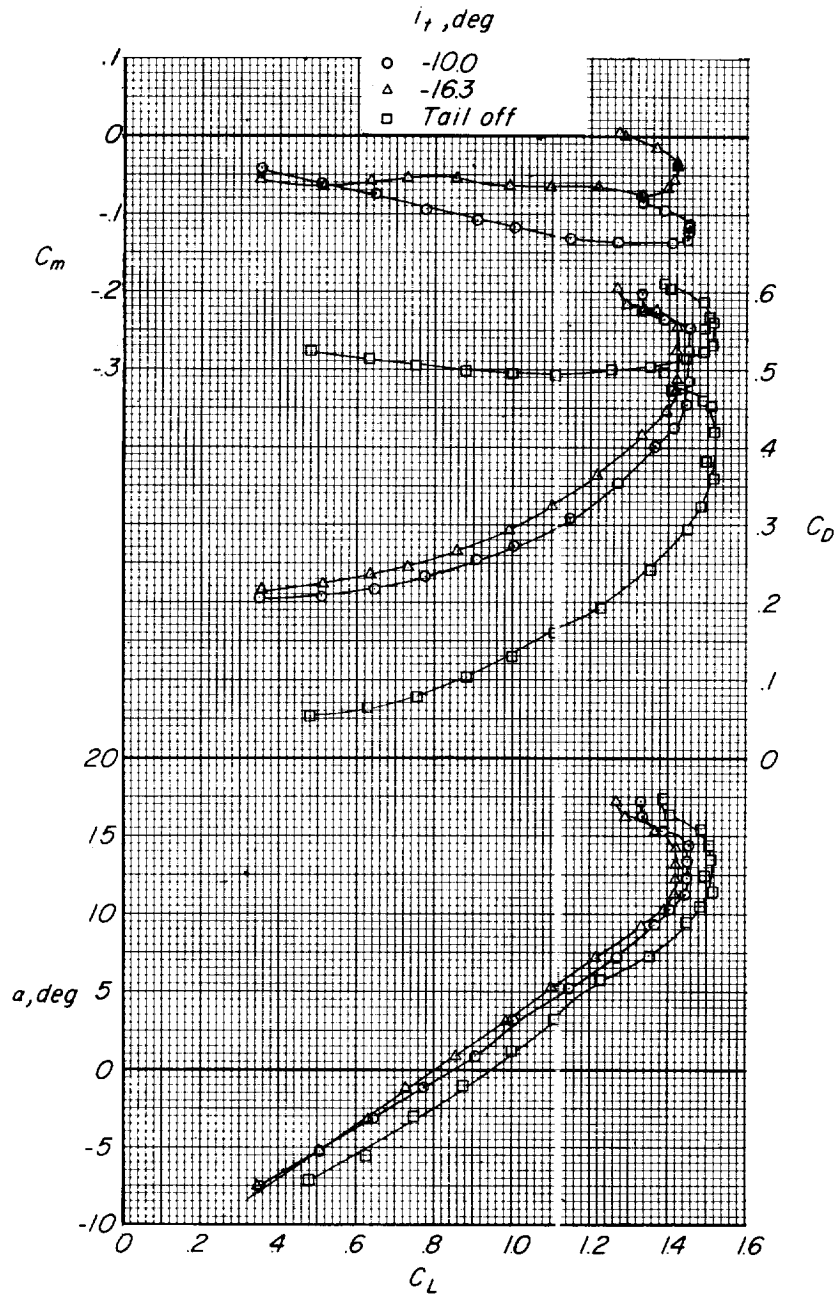
Figure 22.- Effect of horizontal-tail incidence on static longitudinal
aerodynamic characteristics of model equipped with a combination of
single slotted and double slotted flaps. β = 0°; δ_n = 0°; tanks
off; engine nacelles at 0°; wing slats on; q $\approx$ 28 lb/sq ft; δ_f = 26°
for single slotted flap extending from 0.074b/2 to 0.397b/2;
δ_f = 53° for double slotted flap extending from 0.397b/2 to 0.751b/2.
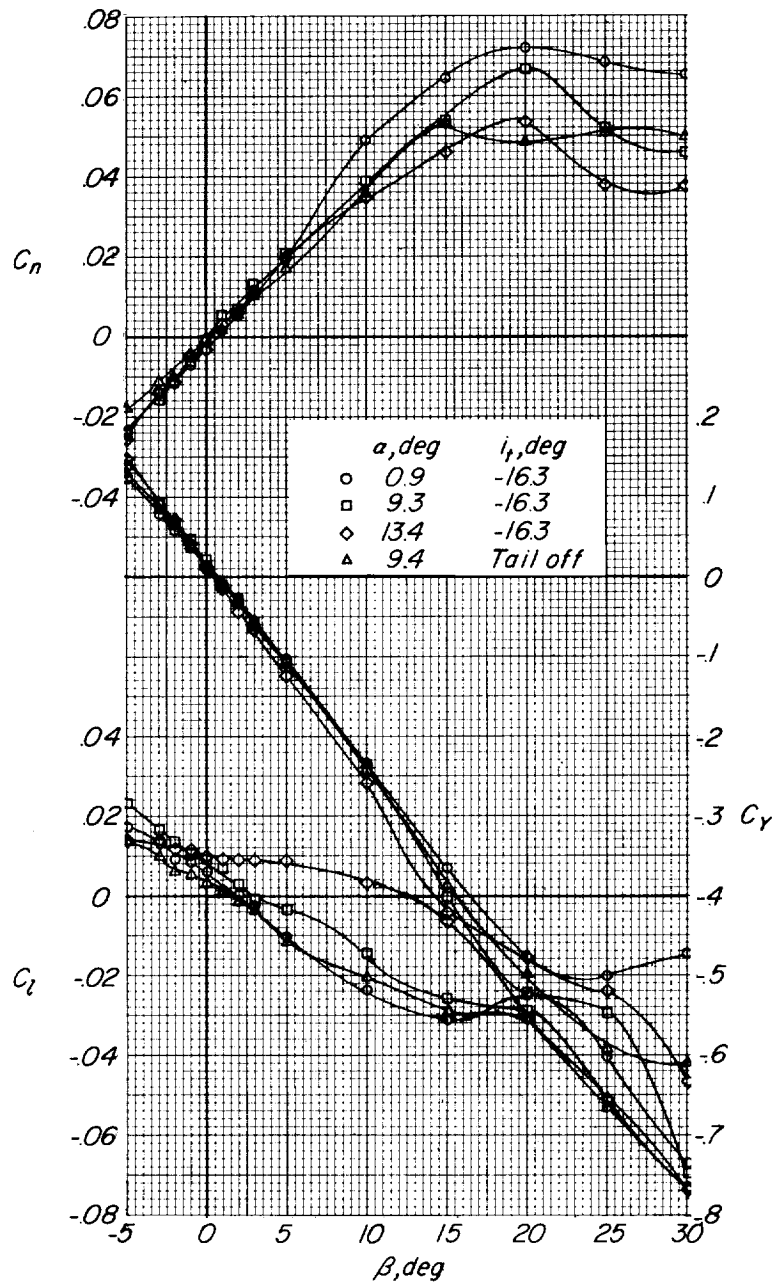
Figure 23.- Effect of angle of attack on static lateral aerodynamic char-
acteristics of model equipped with a combination of a single slotted
and a double slotted flap. $\delta_n = 0^\circ$; wing nacelles at 0°; wing slats
on; $q \approx 28$ lb/sq ft; $\delta_f = 26^\circ$ for single slotted flap extending from
0.074b/2 to 0.397b/2; $\delta_f = 53^\circ$ for double slotted flap extending
from 0.397b/2 to 0.751b/2.
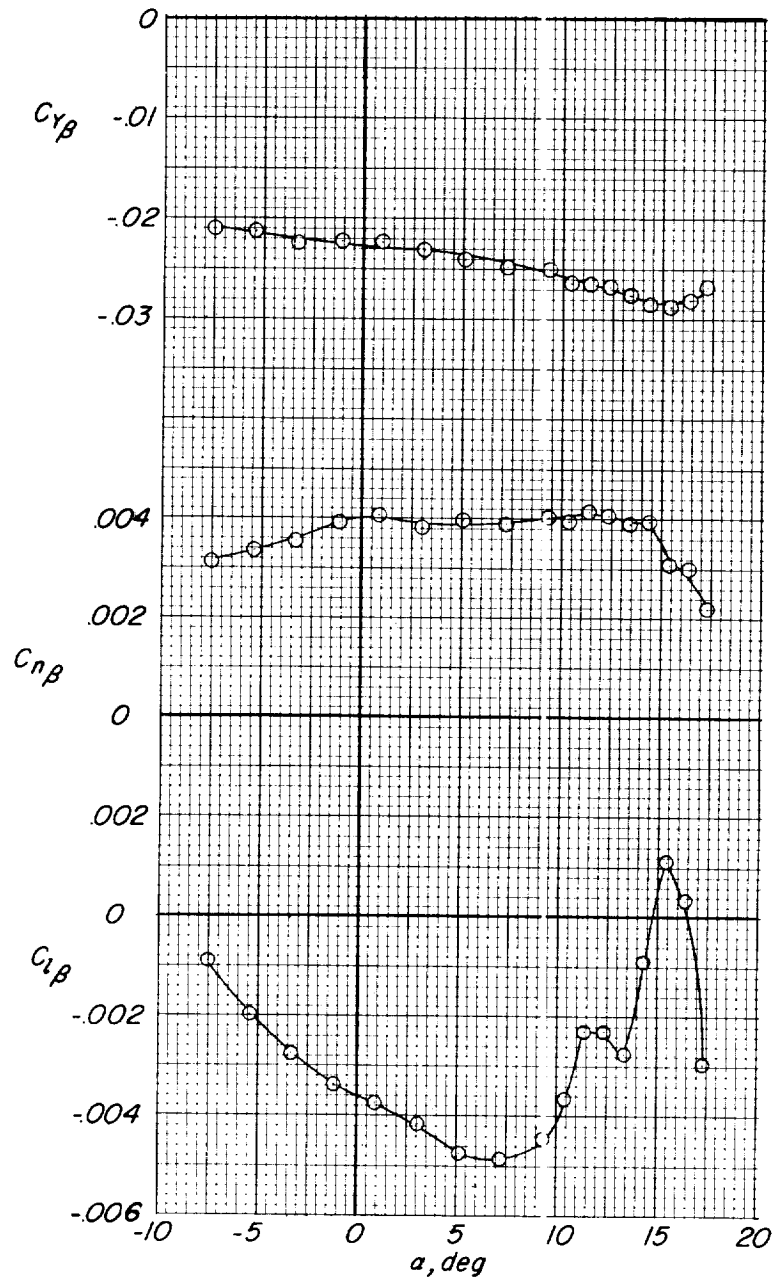
Figure 24.- Variation of the static lateral stability derivatives with angle of attack of the model equipped with a combination of a single slotted and a double slotted flap. $i_t = -16°$; $\delta_n = 0°$; wing nacelles at $0°$; wing slats on; $q \approx 28$ lb/sq ft; $\delta_f = 26°$ for single slotted flap extending from $0.074b/2$ to $0.397b/2$; $\delta_f = 53°$ for double slotted flap extending from $0.397b/2$ to $0.751b/2$; $\beta = \pm 4°$.

7Z

Configuration	δ_f, deg	Slats	
Basic model	0	Off	————————
Short-span inboard double slotted flap	55	Off	————————
Medium-span inboard double slotted flap	50	Off	——— — —— • ——
Medium-span outboard double slotted flap	49	Off	——— — — ——— — —
Medium-span outboard double slotted flap	53	On	——— —— ——— — —
Midspan double slotted flap	42	On	——— —— — —— ——
Full-span single slotted flap	31	On	——— — —— — — ——
Combination of single slotted and double slotted flaps	26, 53	On	——— —— ——— — —
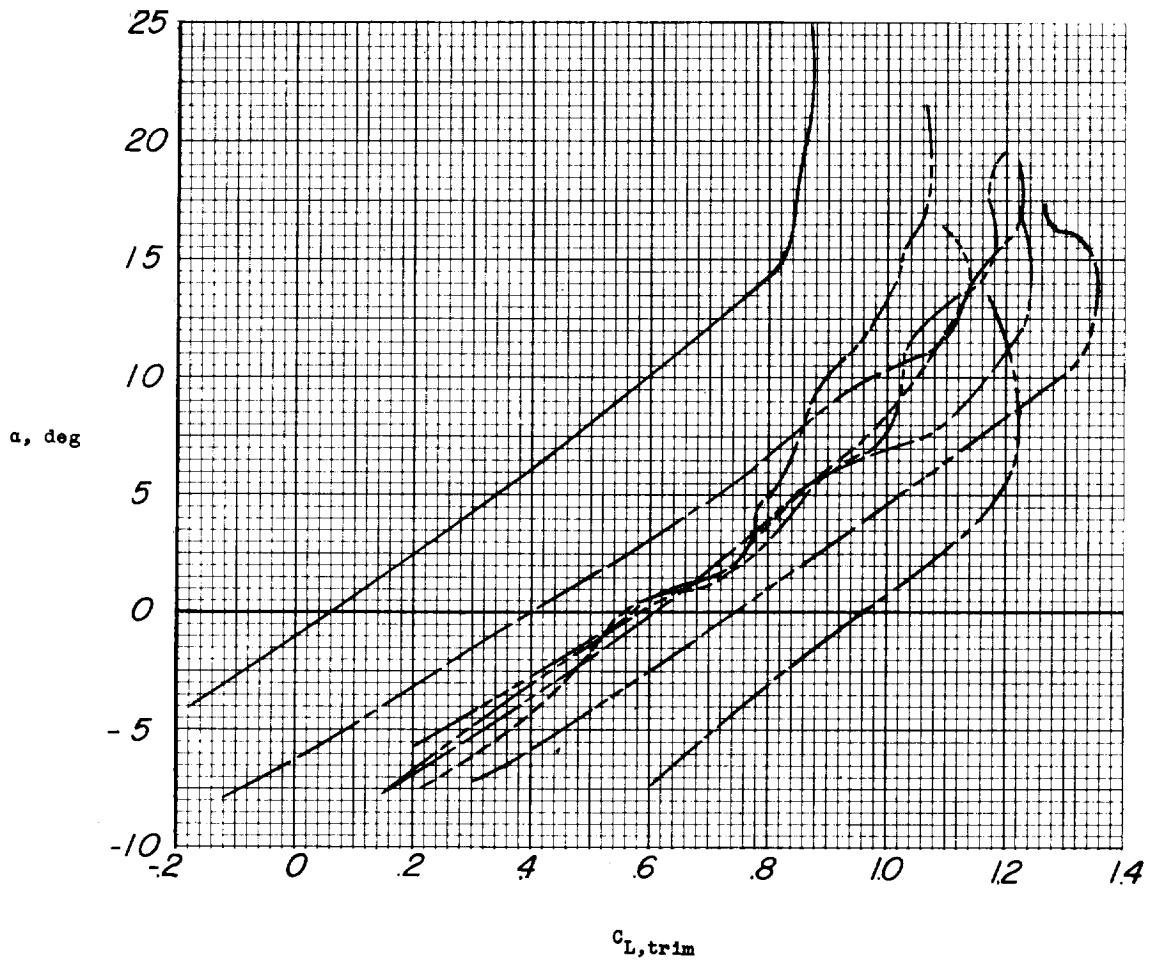
Figure 25.- Variation of angle of attack with estimated trim lift coefficient for basic model and for model with various flap configurations.
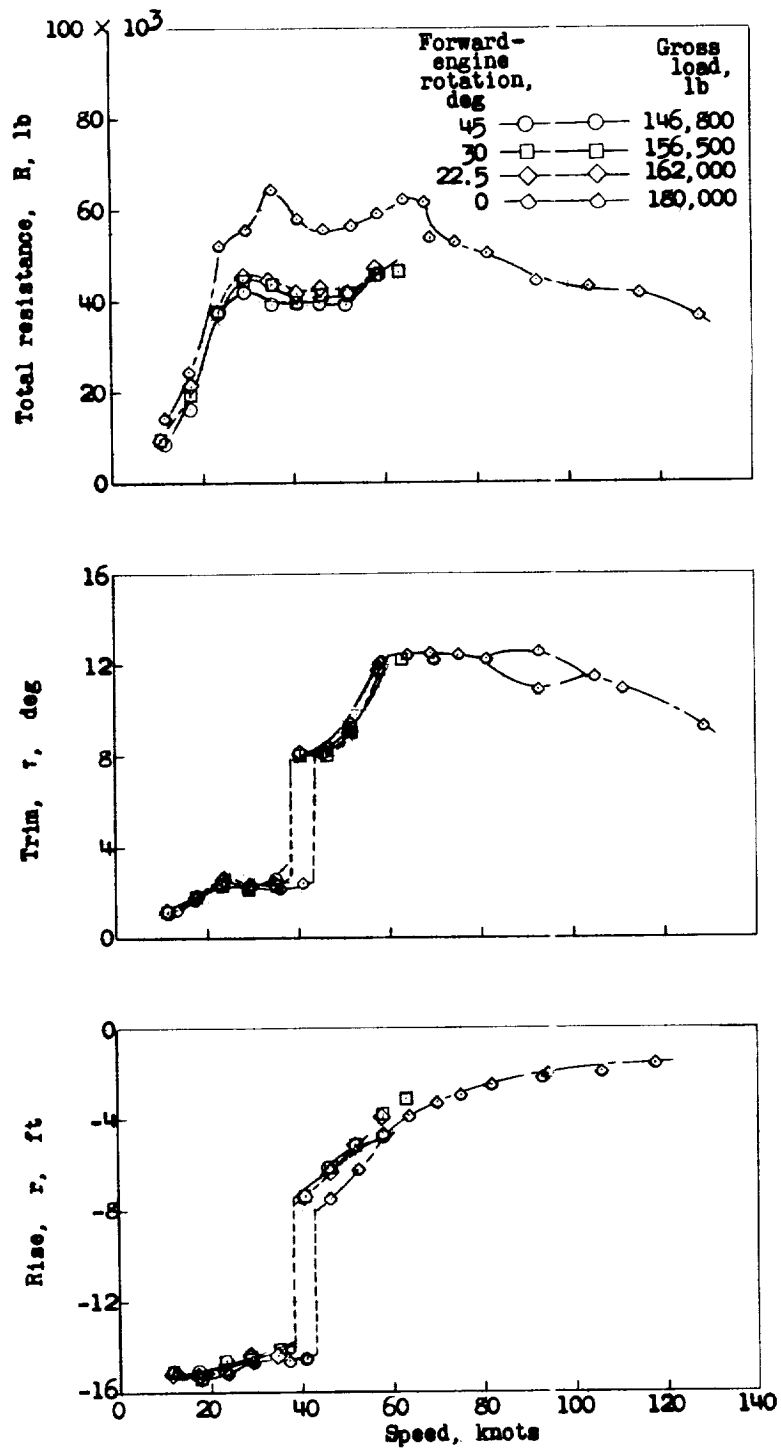
Figure 26.- Effect of engine rotation upon total resistance, trim, and rise. Basic hydro-ski; $\delta_f = 0°$; $\delta_s = 0°$; $\delta_e = 0°$.
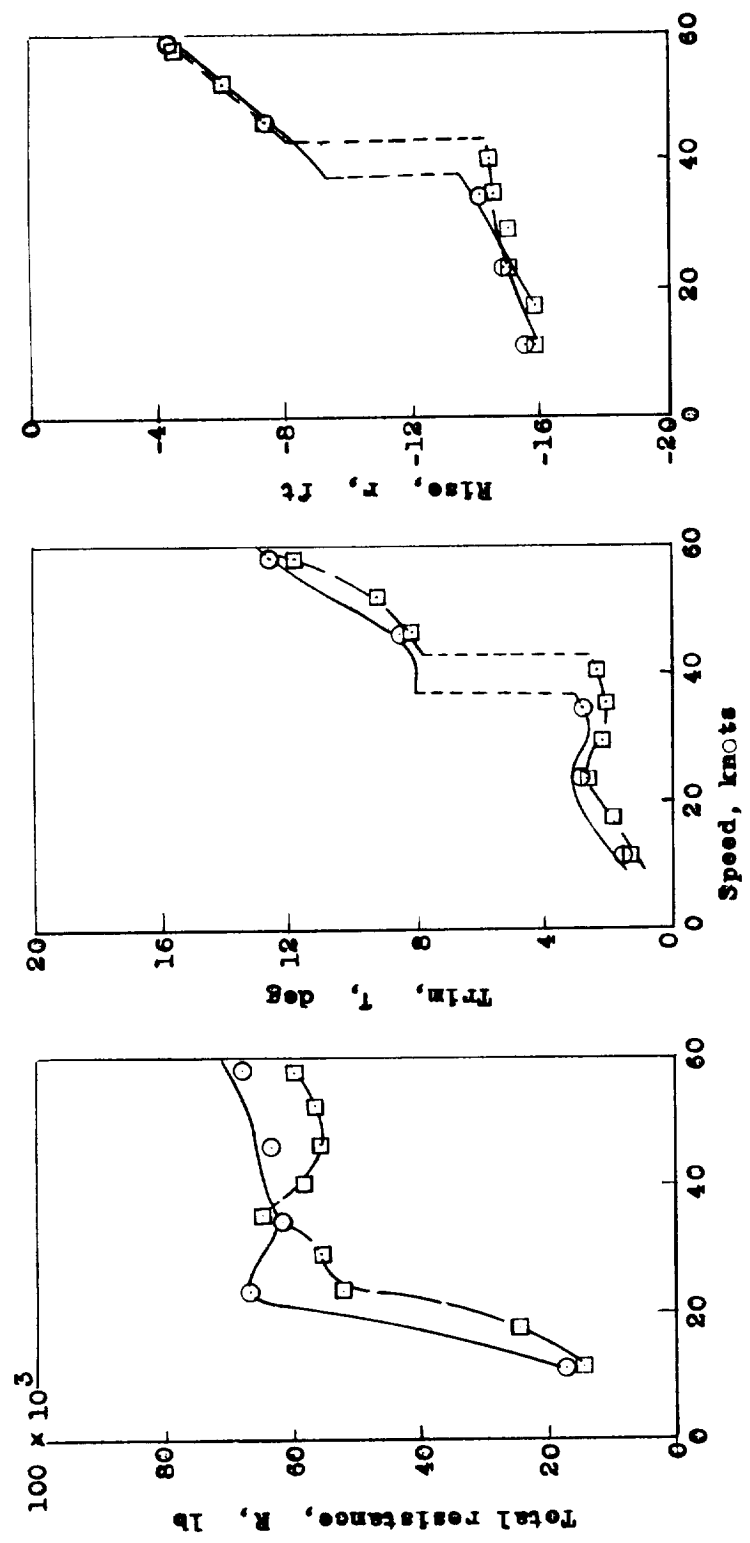
Figure 27.— Effect of external wing tanks upon total resistance, trim, and rise. Basic hydroski; $\delta_f = 0^\circ$; $\delta_s = 0^\circ$; $\delta_e = 0^\circ$.

52
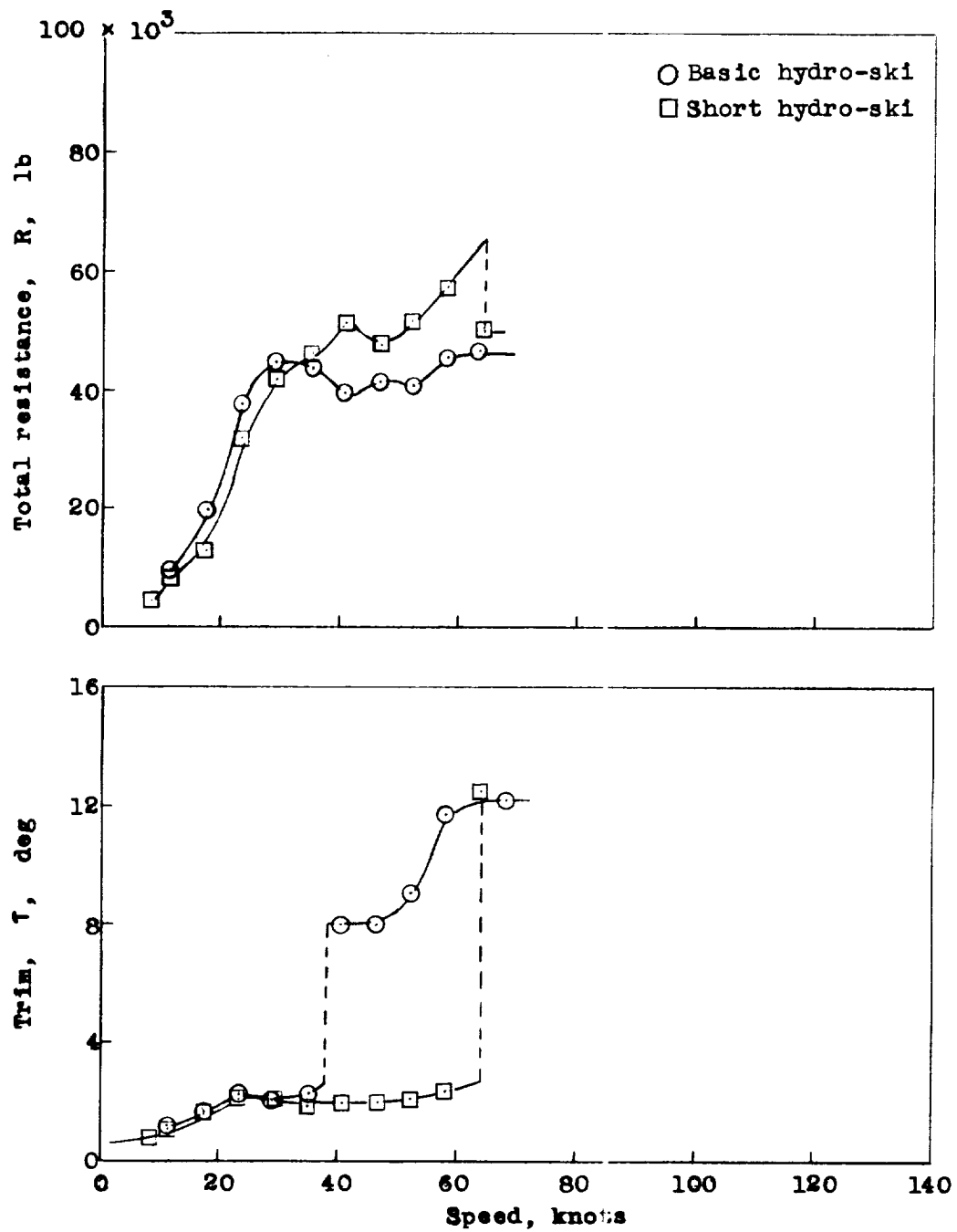
Figure 28.- Effect of hydro-ski size upon total resistance and trim. Gross load, 180.000 pounds; engines rotated 30°; $\delta_f = 0^{\circ}$; $\delta_s = 0^{\circ}$; $\delta_e = 0^{\circ}$.
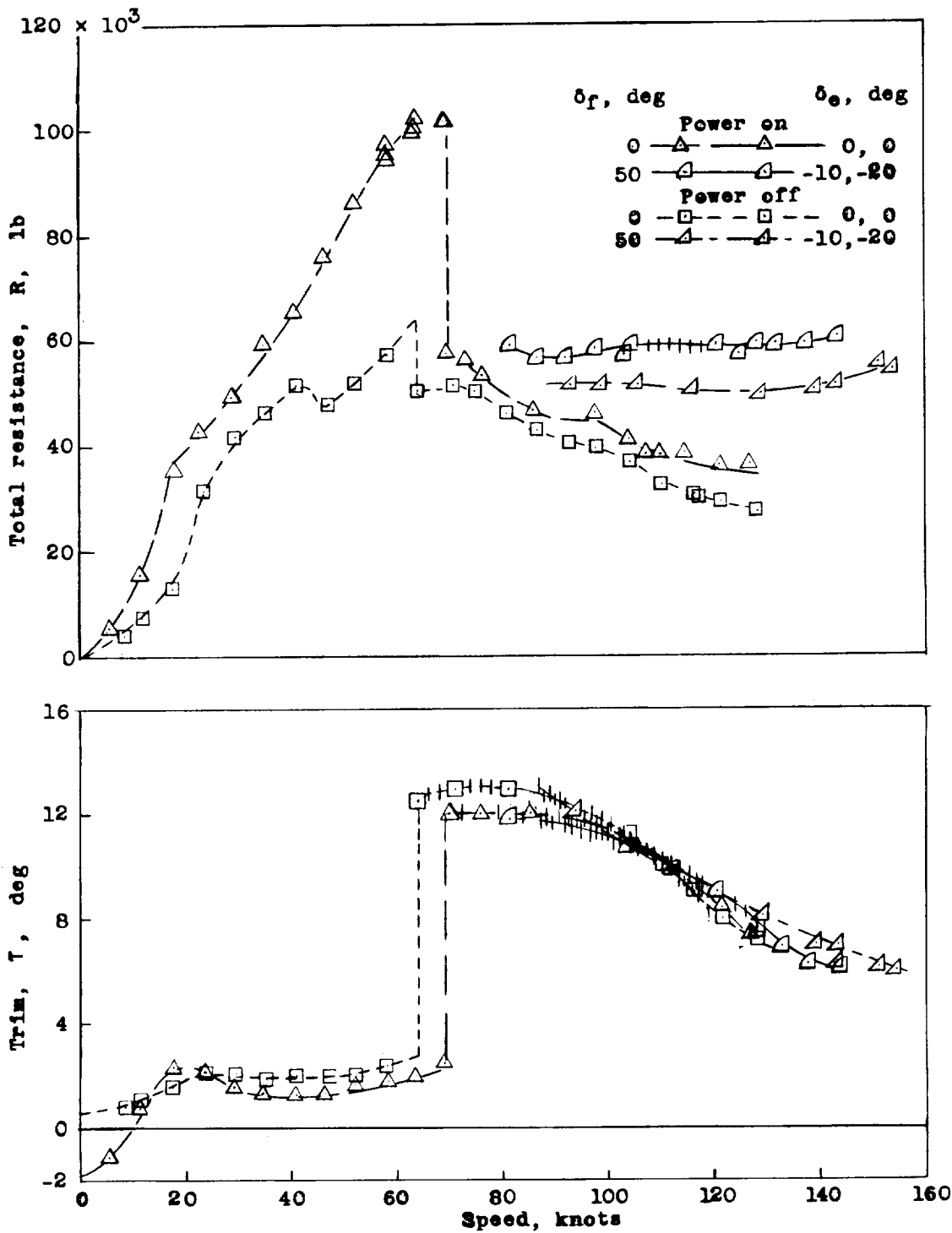
Figure 29.- Effect of power upon total resistance and trim. Gross load, 180,000 pounds; short hydro-ski.
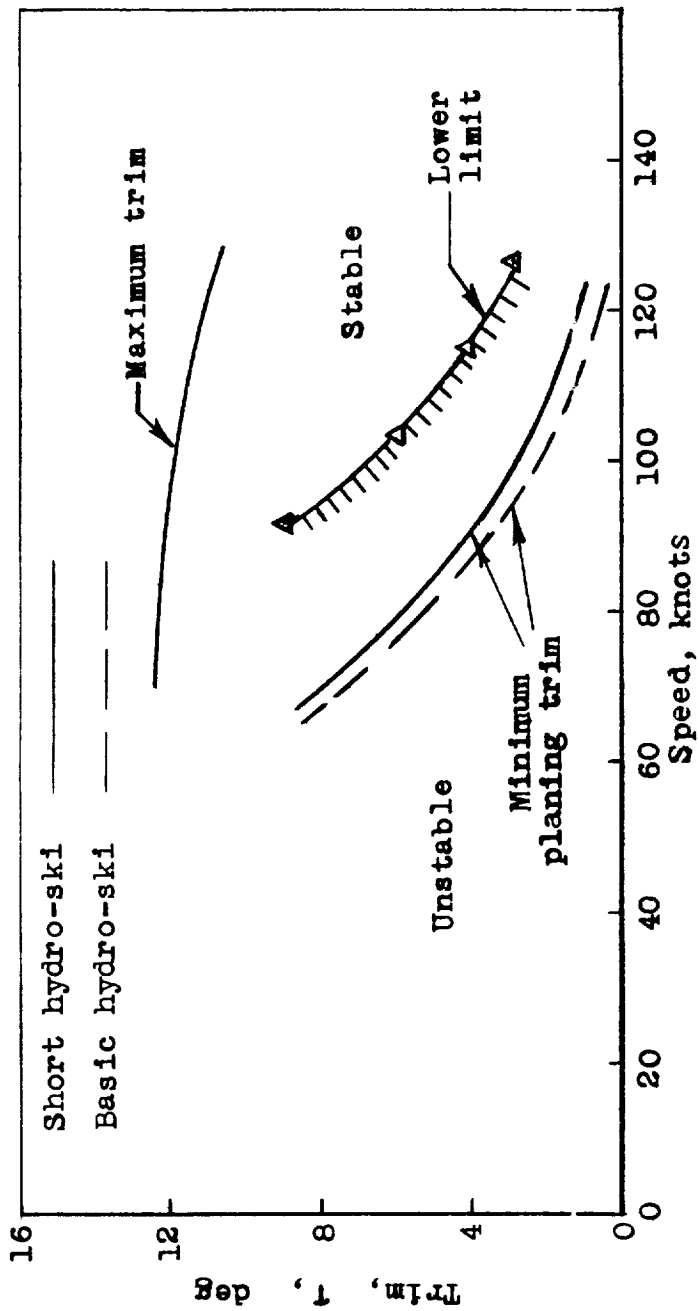
Figure 30.- Trim limits of stability. Gross load, 180,000 pounds; $\delta_f = 0^\circ$.
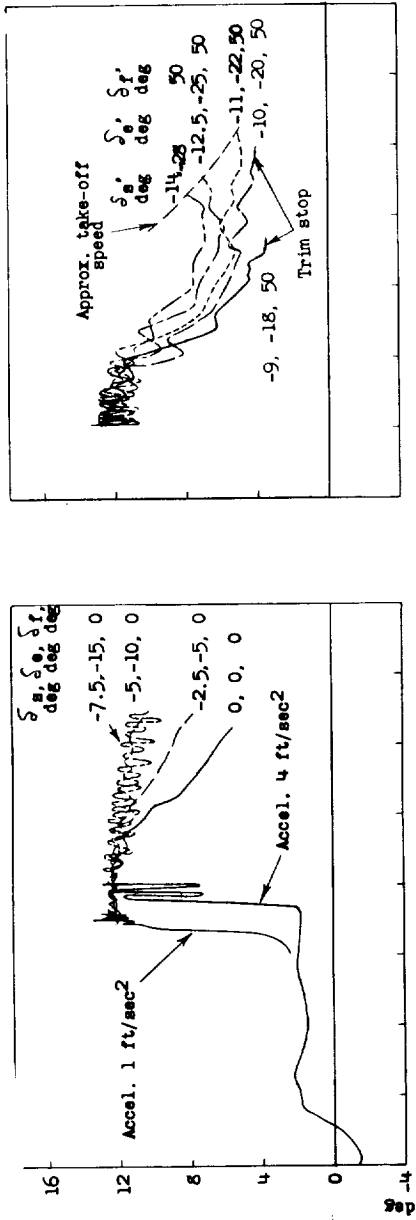
(a) Power on.
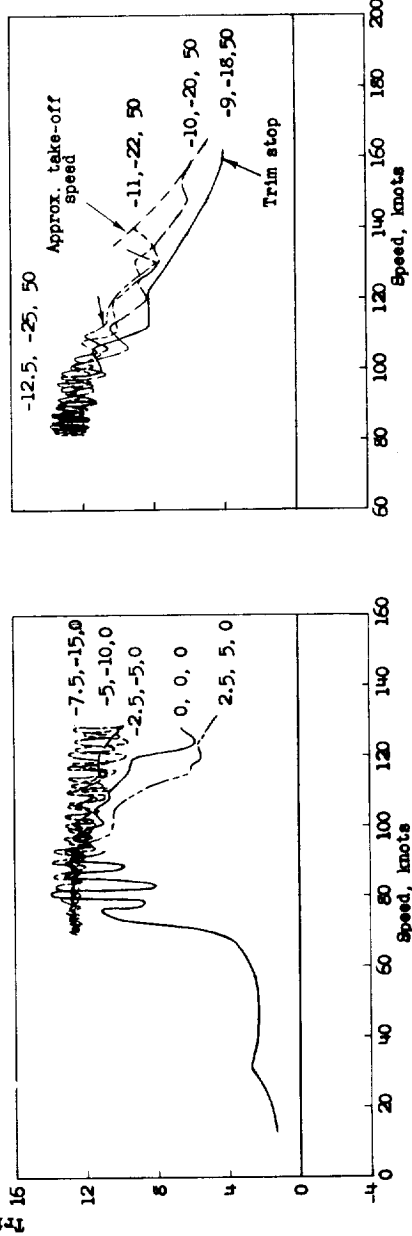
(b) Power off.

Figure 31.- Variations in trim during smooth-water take-offs for various tail deflections.
Gross load, 180,000 pounds; $\delta_f = 0°$ and $50°$.
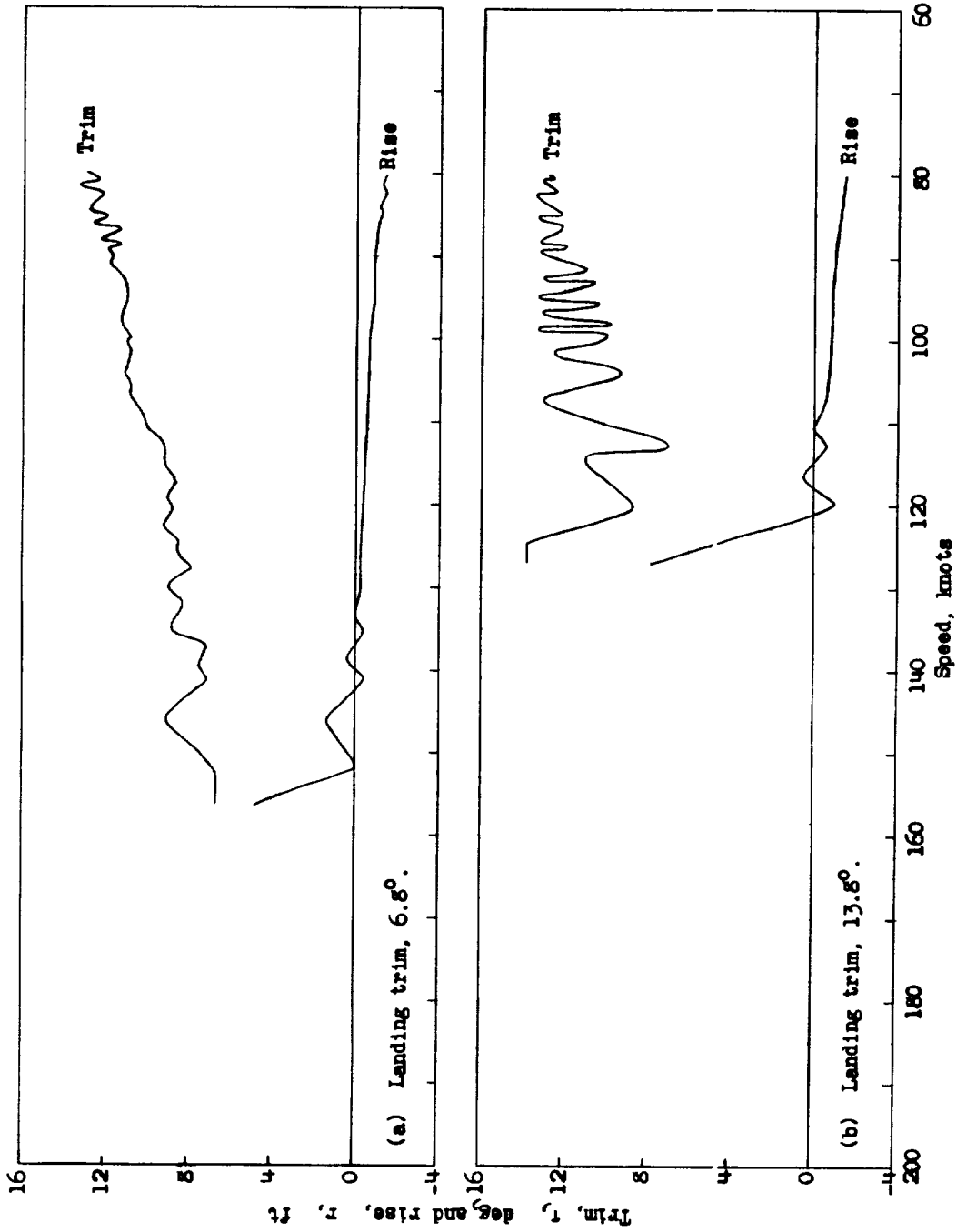
Figure 32.- Variation in trim and rise during typical smooth-water landings. Gross load, 180,000 pounds; $\delta_f = 50^o$.
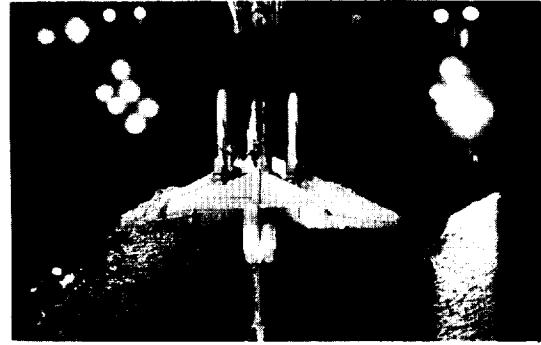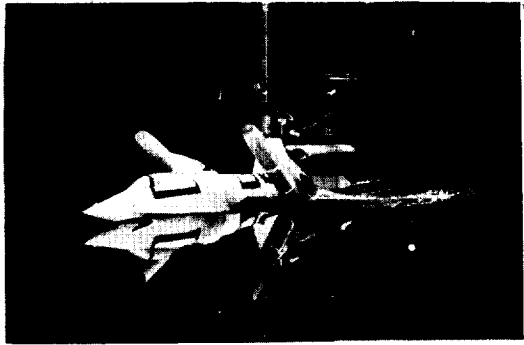
(a) Speed, 11.5 knots.
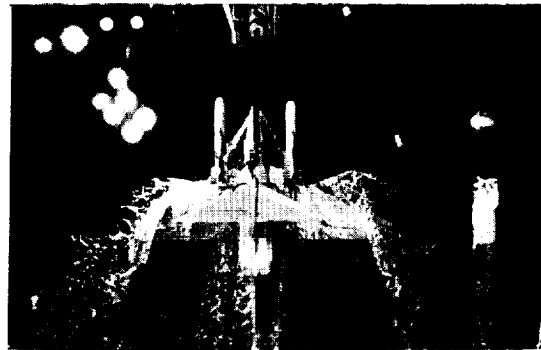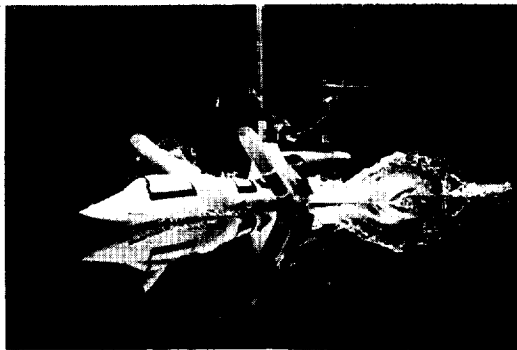
(b) Speed, 23.0 knots.

(c) Speed, 34.5 knots.

L-58-2518

Figure 33.- Spray photographs of model with power off. Gross load, 180,000 pounds.

58
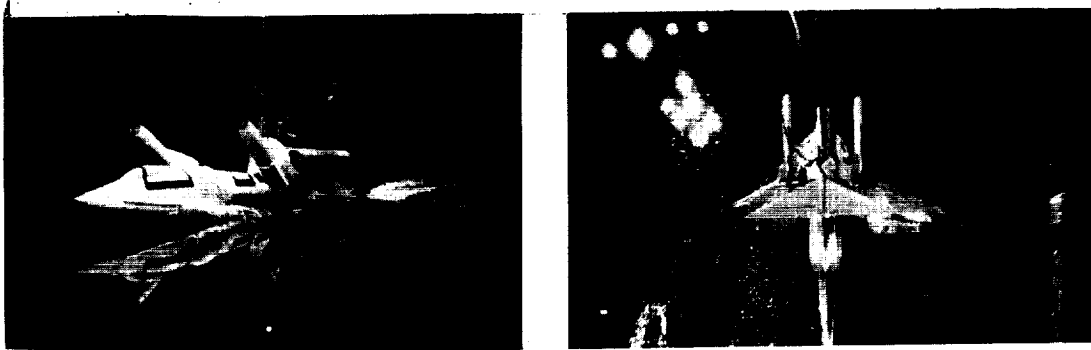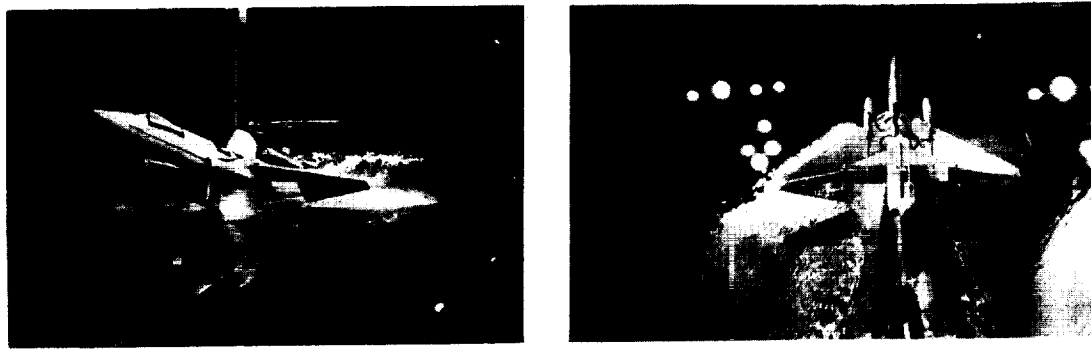
(d) Speed, 57.5 knots.

(e) Speed, 92.0 knots.
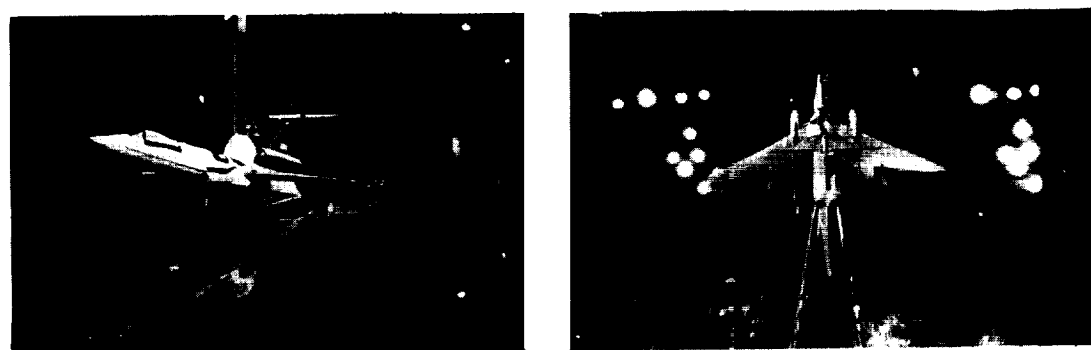
(f) Speed, 138 knots.

Figure 33.- Concluded.   L-58-2519
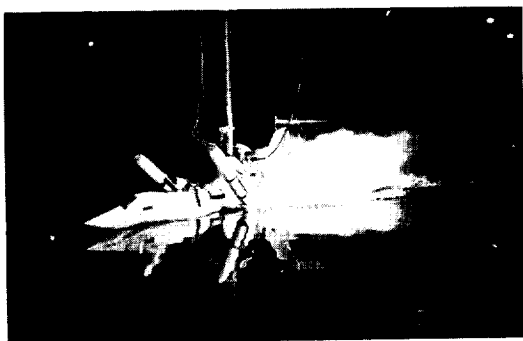
(a) Speed, 11.5 knots.
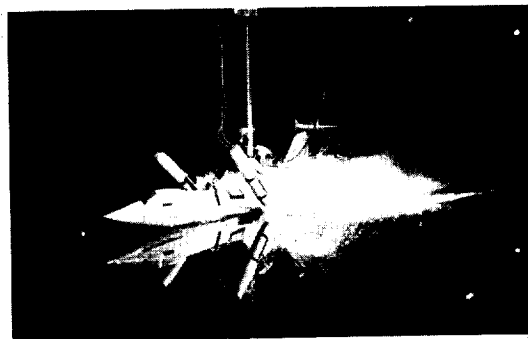
(b) Speed, 23.0 knots.
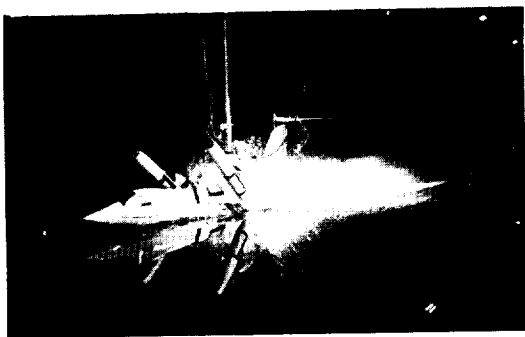
(c) Speed, 34.5 knots.
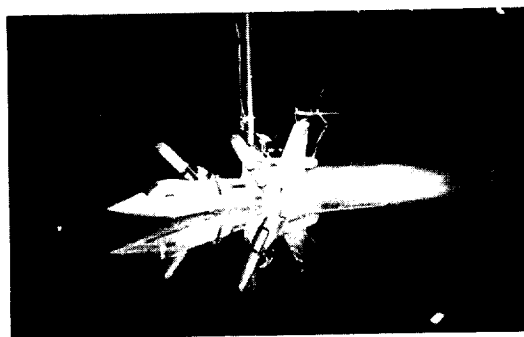
(d) Speed, 57.5 knots.
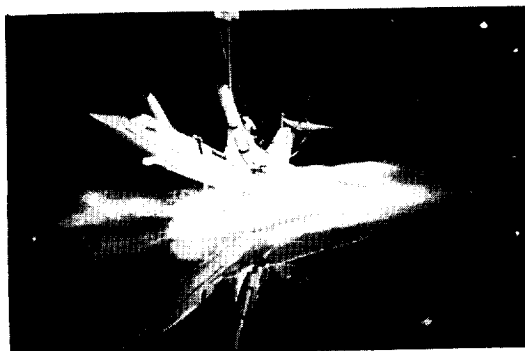
(e) Speed, 69.9 knots.
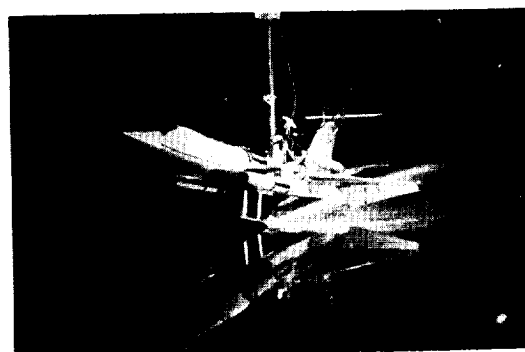
(f) Speed, 115 knots.

L-58-2520

Figure 34.- Spray photographs of model with power on. Gross load, 180,000 pounds.

NASA - Langley Field, Va.